Energy & Environmental Materials WILEY

Recent Developments and Prospects on Functional Graphene-Based Nanocomposites as Potential Sulfur Hosts for Next-Generation Lithium-Sulfur Batteries

*Mohan Raj Krishnan, Chandra Sekhar Bongu, and Edreese Housni Alsharaeh**

Lithium-sulfur batteries have been developing in recent years and appear to offer an alternative to existing commercial batteries that can potentially replace them in the future. With their exceptional theoretical energy density, lower production costs, and affordable and environmentally friendly abundant raw materials, lithium-sulfur batteries have shown the ability to defeat counterparts in the race for rechargeable energy devices currently being developed. The lithium-sulfur batteries display extraordinary features, but they suffer from sulfur's non-conductivity, the shuttle effect that results from polysulfide dissolution, volumetric sulfur changes during charging, and dendrites at the anode, resulting in a decline in capacity and a short battery life. As a result of rigorous and innovative engineering designs, lithium-sulfur batteries have been developed to overcome their drawbacks and utilize their entire potential during the past decade. This review will pay particular attention to porous carbon-based matrix materials, especially graphene-based nanocomposites that are most commonly used in producing sulfur cathodes. We provide an in-depth perspective on the structural merits of graphene materials, the detailed mechanism by which they interact with sulfur, and essential strategies for designing high-performance cathodes for lithium-sulfur batteries. Finally, we discuss the significant challenges and prospects for developing lithium-sulfur batteries with high energy density and long cycle lives for the next-generation electric vehicles.

1. Introduction

Over the past two decades, increasing global energy needs have raised critical concerns about using non-renewable fossil fuels and the associated environmental impacts.[1] Numerous 'clean' renewable energy sources (wind, solar, tidal, and geothermal) exist, but their generation is random and discontinuous.[2] Electrochemical energy storage has been identified as the best solution to address the global energy crisis and its environmental impact.[3] It involves the conversion and storage of renewable energy in electrochemical batteries. For instance, lithium-sulfur (Li-S), Li-ion, sodium-sulfur (Na-S), zinc-air (Zn-Air), and other batteries were developed to offer affordable, clean, and safe energy storage.[4,5] They are widely used in various products, including portable electronic devices, electric tools, automobiles, medical implants, and large-scale smart grids.[6] Gasoline-fueled internal combustion engines are the most significant contributor to the global consumption of non-renewable fuels and environmental damage, so the development of battery-operated electric vehicles (EVs) shows great promise as a sustainable mode of transportation capable of increasing fuel economy and reducing emissions.[7] A massive 41% increase in sales over the previous year and a 5-fold increase in just the past 4 years was recorded by the number of all-electric and plug-in hybrid vehicles sold worldwide in 2023.[8] The growing popularity of EVs has prompted researchers to prioritize their approaches to addressing certain inefficiencies, thus leading to the development of new and high-performance storage systems.[9] Sony Corporation (in 1991) made a significant leap in electrochemical energy storage (EES) when it developed lithium-ion batteries (LIBs), which today command a market share of 63% worldwide among the plethora of electrochemical energy storage technologies.[10] LIBs have evolved into highly reliable EES devices over the last 10 years due to their specific energy, energy density, and cycle stability.[11] LIBs have been widely applied not only to stationary power storage systems but also to portable electronics. Despite this, LIB-enabled EVs are continually failing to meet the rising transportation market expectations since 1) they lack energy density (350 Wh kg^{-1} according to insertion chemistry); 2) lithium is in short supply and extremely expensive; 3) transition metal oxides generated by lithiation are toxic; and 4) they lose performance after 300 cycles.[12] As a result of these factors, the LIBs have reached their finite energy density limits, and the development of new and innovative, low-cost EES systems with high energy density is underway for the next generation of EVs.[13]

The lithium-sulfur battery (LiSB) has emerged as a promising energy storage system and has been considered a low-cost alternative to lithium-ion batteries (**Figure 1**).[14] Compared to LIBs, the LiSBs, with their intrinsic advantages of high specific capacity of sulfur in LiSBs (162 mAh g^{-1} theoretically), which, when combined with lithium anodes (theoretically 3862 mAh g^{-1} theoretical capacity), yield a gravimetric energy density almost 10 times higher than that of LIBs

Dr. M. R. Krishnan, Dr. C. S. Bongu, Prof E. H. Alsharaeh
College of Science and General Studies, AlFaisal University, P.O. Box 50927, Riyadh 11533, Saudi Arabia
E-mail: ealsharaeh@alfaisal.edu
The ORCID identification number(s) for the author(s) of this article can be found under https://doi.org/10.1002/eem2.70032.

DOI: 10.1002/eem2.70032

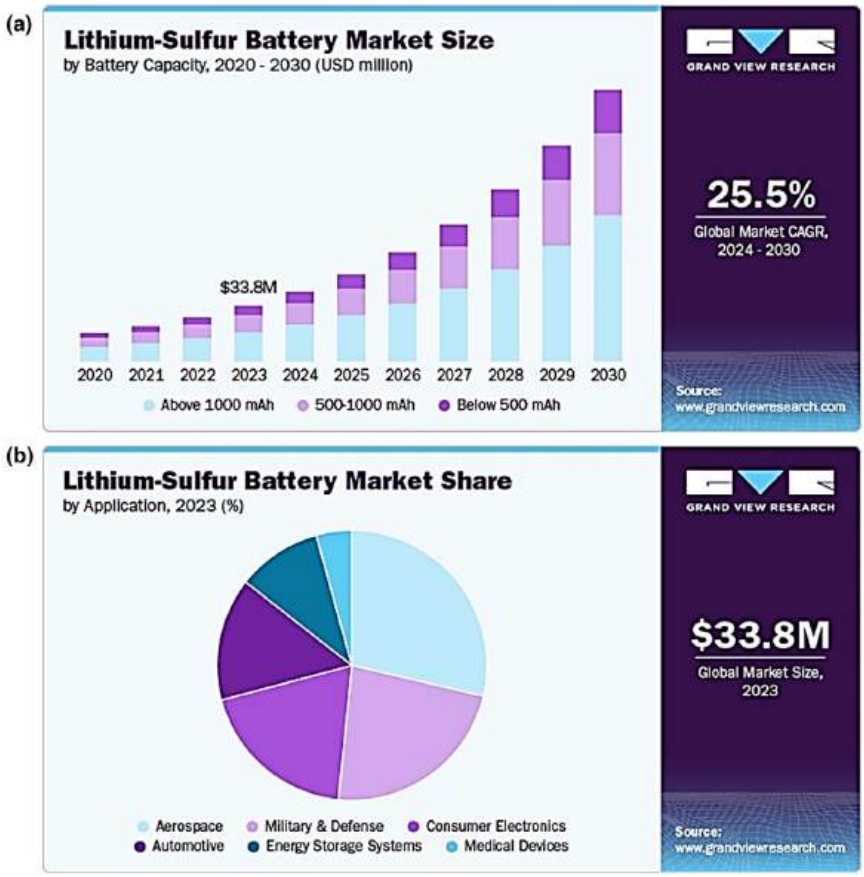

Figure 1. Current Li-S battery market size and market forecast from 2024 to 2030 (Source: Grand View Research). Copyright 2024, Grand View Research.

(2600 Wh kg^{-1}).[15] Sulfur is also an abundant, environmentally friendly, and biocompatible material. Moreover, it is considerably less expensive than LIB cathode materials (lithium carbonate costs \$13 000 ton^{-1}, cobalt costs \$33 000 ton^{-1}, and nickel costs \$14 000 ton^{-1}). In addition, lithium secondary batteries have the most commercial potential and research value because of their safety and reliability.[16]

LiSBs, however, have some issues that need to be resolved before they can be commercially applied:[17]

1 *Limited sulfur loading*:[18] Lower sulfur loadings below the ideal range of 41–70% reduce the capacity of LiSBs.
2 *Lower sulfur utilization*:[19] The room-temperature conductivity of sulfur is very low (5×10^{-30} S cm^{-1}), and therefore, the sulfur cathodes cannot effectively accept electrons in the collector, and their theoretical capacity is hardly achieved since sulfur is not utilized sufficiently.
3 *Volumetric expansion/shrinkage*:[20] A discharged product of S and lithium polysulfides (LiPSs) in LiSBs have densities of 2.03 and 1.66 g cm^{-3}, respectively, indicating that the sulfur cathode expands and shrinks by as much as 80% during electrochemical reactions, adversely affecting the battery integrity and permanently reducing capacity.
4 *Shuttle effect*:[21] Sulfur-based cathodes produce polysulfides (PSs) that would easily dissolve in the electrolyte and diffuse to the lithium anode, forming LiPSs. As a result, even though LiSBs possess an energy density of 3–4 times higher than LIBs (580 Wh kg^{-1}), only a fraction of the theoretical energy density is usually achieved. As a result of these factors, their cycling stability is inferior, they suffer from capacity loss, they use little sulfur, the lithium anode corrodes, and they suffer from severe self-discharge, which makes it difficult to penetrate the market. Numerous measures have been implemented to design high-performance LiSBs, such as confined sulfur in host materials, modified separators, hybridized interlayers, and new electrolytes. LiSB energy density and life cycle have been drastically improved by shuttle inhibition using porous host materials such as porous carbon,[22] molecular organic frameworks (MOFs),[23] aerogels,[24] etc. LiPSs are chemically/physically anchored within porous host materials and are not soluble in electrolytes because of their chemical/physical attraction.

Nazar et al. pioneered sulfur encapsulation in porous materials.[25] The authors demonstrated successful encapsulation of sulfur molecules in the ordered pore channels of mesoporous carbon (CMK-3). The sulfur confinement in a porous host material of CMK-3 resulted in a substantial increment in the respective LiSB's specific capacity, rate performance, and cycle life. After this groundbreaking work, the LIBs have gained intense research interest, and significant advances have been made.[1] During the last decade, sulfur cathodes have been the subject of an exponential increase in scientific publications, demonstrating their considerable interest.[26] Numerous design strategies have been proposed to realize the LiSBs at the industrial scale, including the design of host materials, separator modification, the optimization of electrolytes, and the protection of lithium.[27,28] It is highly desirable that a host material possesses high conductivity, high porosity, and strong encapsulation capability.[29] Encapsulating sulfur in porous conducting host materials offers a range of advantages in LiSBs, such as high sulfur loading, conductivity enhancement, fast ion transport, inhibition of the shuttle effect through effective anchoring of PSs, acting as a buffering zone to compensate for the volumetric change, and high electrocatalytic activity, which increases kinetics and reduces dissolution of LiPSs at the same time, accelerating LiPSs conversion.[23]

Several host matrix materials were proposed and critically investigated for S cathode due to their critical advantages in high-performance LiSB design. Porous materials such as graphene, carbon nanotubes, mesoporous carbon, MOFs, and covalent organic frameworks (COFs) have been extensively studied in recent years to fabricate sulfur-based cathode materials.[23] Comparing the host matrices based on inorganic materials, porous carbon-based host materials are distinguished by high conductivity, porosity, and specific surface area with tunable pore size

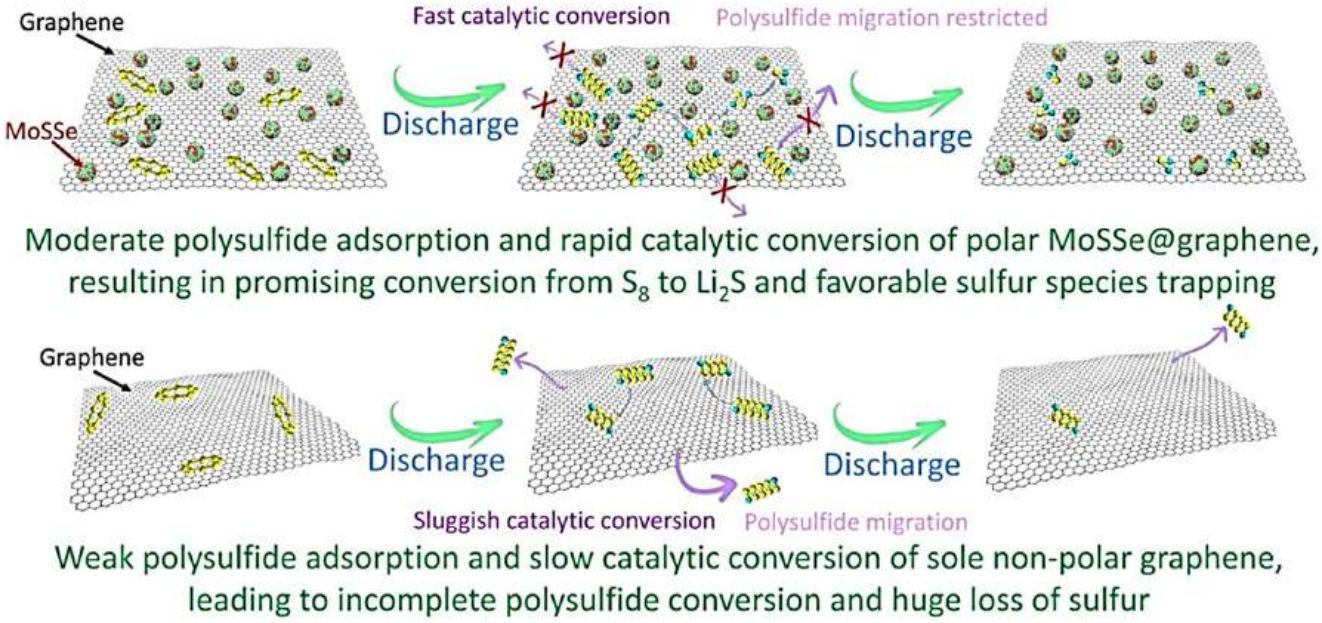

Figure 2. MoSSe@graphene composites for long-cyclable Li-S batteries.[36] Copyright 2025, Elsevier

distributions.[30] Moreover, the porous carbon materials can be easily doped, co-doped, and functionalized to effectively create heterostructures to tune their electric and structural properties.[31] Therefore, the porous carbon-based hosts with large pore volumes can efficiently limit the dissolution of LiPSs by trapping them within their frameworks, ensuring high sulfur loading and facilitating surface interactions like adsorption and catalysis.[32] Various carbon nanostructured host matrixes have been reviewed recently for their potential as sulfur confinement and polysulfide anchoring materials in LiSBs.[33–35] However, a comprehensive comparison of carbon-based hosts for immobilizing sulfur in LiSBs is still lacking. Furthermore, none of the reviews have examined the different subtypes of a particular material, especially graphene-based ones. This review aims to provide a comprehensive overview of the current state of graphene-based hosts for sulfur cathodes in LiSBs and provide insight into innovative electrode design routes to promote LiSB commercialization.

2. Graphene-Based Nanocomposites as Potential Sulfur Hosts for Next-Generation LiSBs

This section critically summarizes various graphene-based nanocomposites as potential host materials for high-performance LiSBs. Wei et al.[36] reported a sulfiphilic few-layer molybdenum seleniosulfide (MoSSe) nanoflakes decorated on graphene (MoSSe@graphene), a two-dimensional and catalytically active heterostructure composite (**Figure 2**). A facile microwave method was used to prepare this conceptually new sulfur host, assisting LSBs to accelerate at the interfacial level. The sulfiphilic MoSSe nanoflake has a strong interaction with soluble polysulfides, and this interaction dynamically promotes polysulfide redox reactions. Furthermore, graphene nanosheets provide a physical barrier that mitigates the diffusion of lithium polysulfides and enables much more uniform sulfur distribution, which inhibits polysulfide shuttling while accelerating sulfur conversion reactions. This resulted in superior rate performance (1091 mAh g^{-1} at 1 C) and an ultra-low decay rate of 0.040% per cycle after 1000 cycles.

In another recent study, Wei et al.[37] reported growing $MoTe_2$ nanosheets on graphene using ultrafast and simple microwave-assisted chemical coupling and heating methods to develop hybrid sulfur host materials for Li-S batteries (**Figure 3**). With excellent electrocatalytic activity, $MoTe_2$ nanosheets and highly conductive graphene form a nano reservoir to contain sulfur and intermediate polysulfide species and accelerate electron transfer. Accordingly, Li-S batteries with $MoTe_2$@graphene@carbon cloth electrodes displayed excellent cycle stability (98.7% capacity retention after 100 cycles at 0.2 C) and excellent rate performance. By combining the chemical affinity and electrocatalytic ability of polar $MoTe_2$ with graphene and freestanding carbon cloth, polar $MoTe_2$ can be used as a host material to mitigate the shuttling effect in rechargeable lithium-ion batteries through effective physical confinement.

Lan et al.[38] report the development of a chip-inspired LSB cathode featuring a vertically integrated structure implanted with Mo_2C nanoparticles and nano-sulfur into graphene to act as the cathode (**Figure 4**). This configuration allowed for synthesizing sulfur nanoreactors (SNRs) assembled into a tandem array on graphene—generating integrated LiSBs. Through spatial confinement and protection of the S-NRs, polysulfides were prevented from dissolving, diffusing, and losing, thereby enhancing sulfur utilization and redox reaction kinetics. Nanoreactor units can be combined in tandem, isolated, and multiplied synergistically to enhance adaptability. This resulted in an integrated LSB cathode achieving excellent electrochemical properties with an initial capacity of 1392 mAh g^{-1} at 0.1 C, a low capacity decay rate of 0.017% per cycle during 1500 cycles at 0.5 C, and a superior rate performance. The authors present a rational design and method for developing high-performance energy storage devices that are precise and economical.

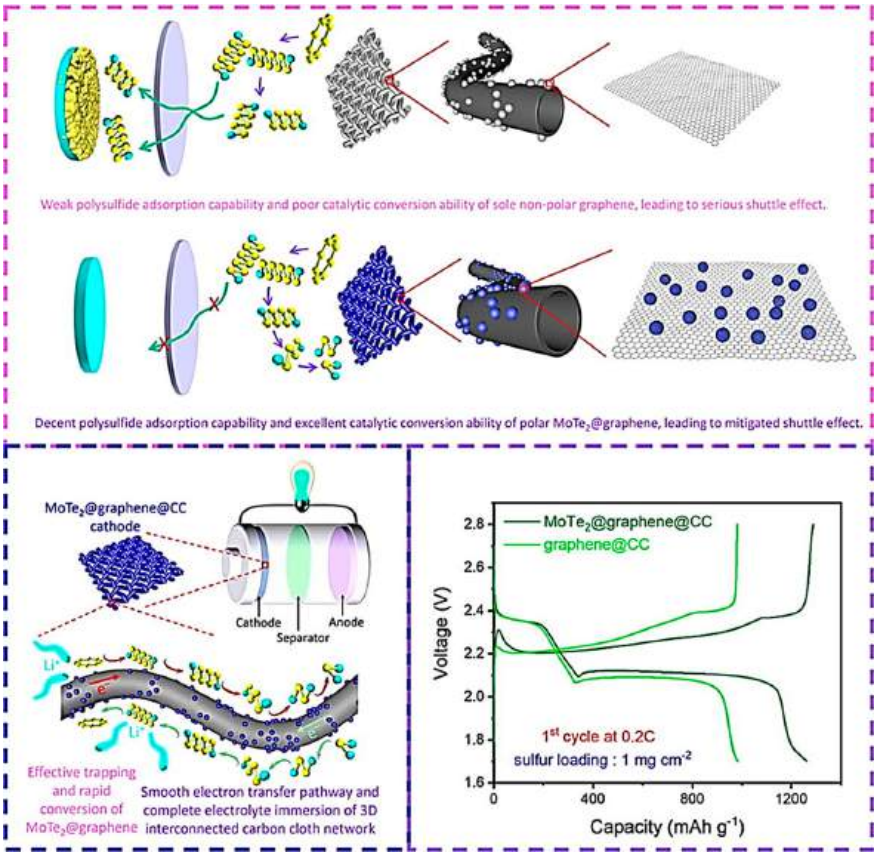

Figure 3. A microwave synthesis of $MoTe_2$@graphene composites that accelerates polysulfide conversion and promotes the nucleation of Li_2S for high-performance Li-S batteries.[37]

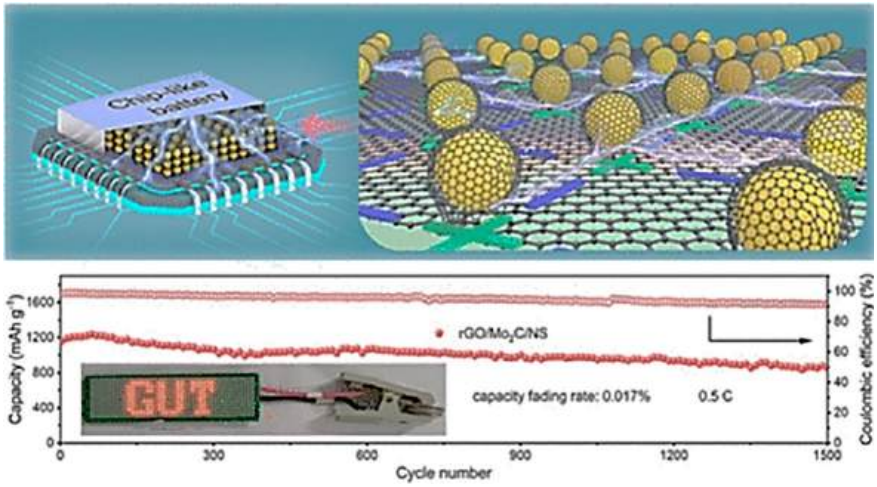

Figure 4. High-performance lithium-sulfur batteries using monodisperse sulfur nanoreactors on graphene.[38] Copyright 2024, American Chemical Society

Using a one-step PS additive reaction at 320 °C, Chuang et al. report high volumetric capacities and high sulfur packing density in phosphorus-sulfur/graphene composites (PS/G composites).[39] A sheet of binder-free LiS cathode can be easily fabricated from PS/G composites that are self-supporting, bendable, and compressible (**Figure 5**).[39] The fabricated PS/G cathode shows an excellent specific capacity of 959 mA h g^{-1} with a low-capacity fading rate (0.15% per cycle) for 200 cycles. Therefore, the electrode has a volumetric capacity of 1726 mA h cm^{-3} (volume is based on the cathode materials and the current collector). It has also been demonstrated that flexible Li-S pouch cells using PS/G composites as cathodes have stable electrochemical characteristics under bending conditions, demonstrating their suitability for commercial batteries.

Ning et al.[40] reported using vanadium oxide (VO_2) nanotubes with a relatively high redox potential (than sulfur) to compound in situ with graphene (G) to create a binary sulfur host for VO_2/G based on the VO_2/G ratio (**Figure 6**). With VO_2 nanotubes in a binary environment, soluble lithium polysulfides (LPSs) can be chemically adsorbed, which improves their electrochemical conversion kinetics. This allows the shuttle effect of LiPSs to be inhibited. Additionally, graphene improves the cathode material's electronic conductivity and reduces the electrode's polarization. It is impressive that the fabricated VO_2/G/S electrode exhibits a high specific capacity, a good rate performance, and excellent cycling stability, which holds great potential for a wide range of applications.

In a study by Ying et al.,[41] Fe–Co sulfide/graphene/CNTs were combined into a functional interlayer composite (FCS@GC) (**Figure 7**). Using the cross-linked 3D network formed by CNTs and graphene, the composite could avoid carbon agglomeration and enhance the physical adsorption capacity of LiPSs, effectively improving the transfer of Li^+/e^-. In addition, the loaded $FeCoS_4$ improves the kinetics and chemical adsorption of LiPSs within the composite, inhibits the shuttle effect at various levels, and enhances the chemical adsorption of LiPSs. LiSBs with FCS@GC as their functional interlayer can achieve 787.5 mA h g^{-1} after 200 charge/discharge cycles at 0.5 C. The capacity of LiSBs with FCS@GC interlayers can still be maintained after 110 cycles at a sulfur loading of 5 mg cm^{-2}. After 800 cycles, the capacity decays at a rate of 0.036% per cycle. Its structure will provide viable solutions for commercializing LiSBs.

By combining the strong adsorptive and catalytic properties of $CoNiO_2$ with the electrical conductivity of Co_4N, Gong et al. demonstrated a synergistic enhancement effect of $CoNiO_2$/Co_4N heterostructures (**Figure 8**).[42] Based on theoretical calculations and experimental design, it can significantly inhibit the shuttle

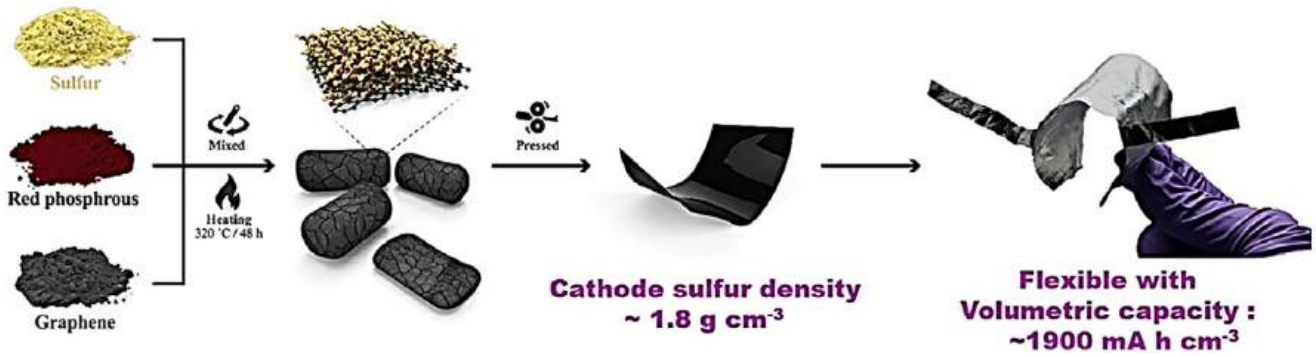

Figure 5. A flexible lithium-sulfur battery cathode made of phosphorus-sulfur/graphene composite with an extremely high volumetric capacity and high performance.[39] Copyright 2020, Elsevier.

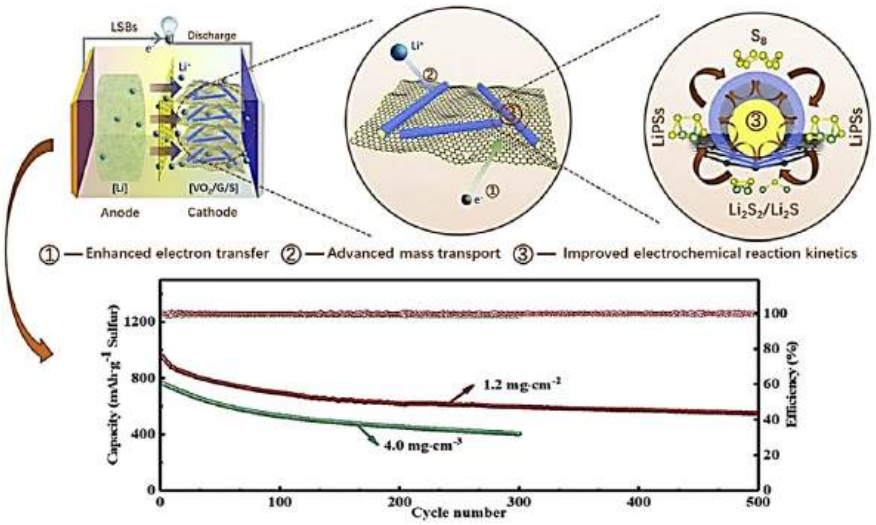

Figure 6. A rational binary sulfur host consisting of VO_2 nanotubes and graphene for the development of superior lithium-sulfur batteries.[40] Copyright 2020, Elsevier.

effect through chemisorption and catalytic conversion of polysulfides and improve ion and electron transport rates. This way, the graphene composite sulfur cathode supported by the $CoNiO_2/Co_4N$ nanowires exhibits improved sulfur species reaction kinetics. The corresponding LiSB exhibited a high-rate capacity of 688 mAh g^{-1} at 4 C with an ultralow capacity fading rate of ≈0.07% per cycle for 600 cycles. The graphene composite structure and heterostructure nanowires provide a new approach for rapid polysulfide capture-diffusion conversion. **Table 1** summarizes recent key works on improved LiSBs with high specific capacity, enhanced rate performances, and increased charge–discharge cycles based on graphene-based nanocomposites for sulfur cathode preparation.

3. Graphene Oxide-Based Nanocomposites as Potential Sulfur Hosts

This section critically summarizes various graphene oxide-based nanocomposites as potential host materials for high-performance LiSBs. Designing sulfur host materials efficiently to address polysulfide shuttling in lithium-sulfur batteries is essential. Using Co@TiO_2 hollow spheres tightly wrapped by graphene oxide (labeled as Co@TiO_2/GO), Zhang et al.[80] constructed a multilayer sulfur immobilizer with a multilevel sulfur storage space (**Figure 9**). In this structure, sulfur was encapsulated on three levels: inside the cavities of the Co@TiO_2 hollow spheres, between the Co@TiO_2 spheres and the GO sheets, and within the interlaminar pores of GO. As a result, the inner and outer surfaces of the Co@TiO_2 hollow spheres were better at participating in the LiPS conversion reactions. Further, incorporating Co nanoparticles and abundant oxygen vacancies enhanced redox reaction kinetics in LiPS. Thus, this multi-level sulfur storage space is beneficial for the storage and blockade of polysulfides and for improving the LiSB's energy storage performance. As a result of these favorable structural characteristics, the initial discharge capacity of Co@TiO_2/GO/S cathode reached 807 mAh g^{-1} at 1 C with a slow decay rate of 0.053% per cycle and a high specific capacity of 552 mAh g^{-1} at 5 C.[80]

Polyaniline-based nanocomposites are promising candidates for hosting sulfur in LiSBs based on cathode materials. An ice-grown PANI-GO-S nanocomposite has been developed by Badi et al.[81] To fabricate the cathode, 1.0 wt% of the prepared nanocomposite was mixed with $LiNi_{0.5}Mn_{0.5}O_2$ and PVDF in *N*-methyl pyrrolidone (NMP) solvent. The cyclic voltammetry of PANI and its nanocomposite shows redox peaks at 1.9 and 2.7 V and oxidation peaks at 2.6 and 2.2 V, which show the transition from Li_2S to S^{2-} and later sulfur elemental S_8. The nanocomposite cathode exhibited a high specific capacity (868 mAh g^{-1}) up to 400 cycles with a coulombic efficiency of 98%. The PANI-GO-S nanocomposite is presented as an innovative approach to fabricating electrodes with a high specific capacity in lithium-based electrochemical charge storage cells.[81]

Ma et al.[82] proposed suppressing the polysulfide diffusion problem and large-volume expansion by loading sulfur inside the wrap while

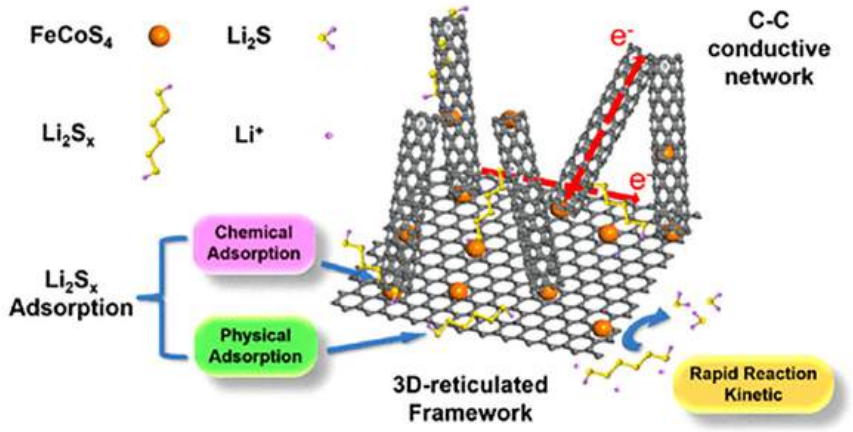

Figure 7. Three-dimensional reticulated Fe–Co sulfide/graphene/CNTs composites as functional interlayer capturing and converting polysulfide for high-performance lithium–sulfur batteries.[41] Copyright 2024, American Chemical Society.

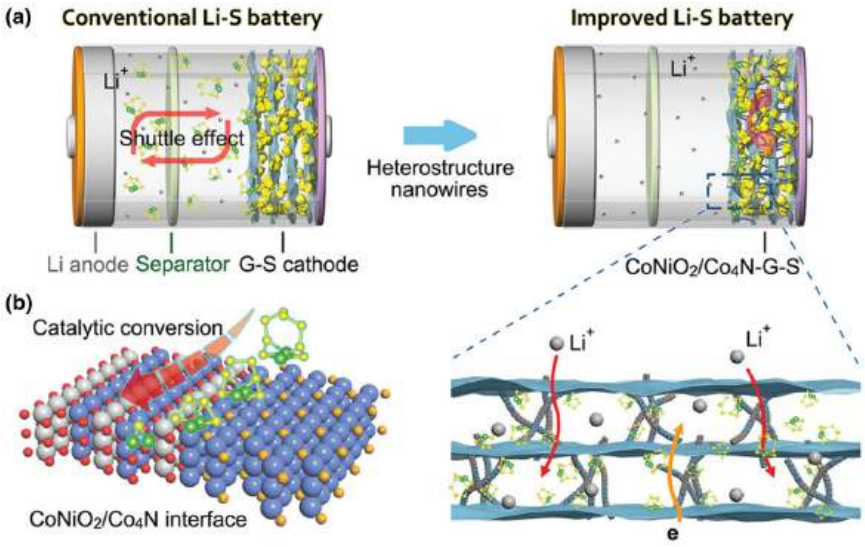

Figure 8. a) A comparison of the conventional LiSB with the "shuttle effect" and the $CoNiO_2/Co_4N$-based improved cell. b) Schematic illustration of interface mechanism of heterostructure and polysulfides.[42] Copyright 2022, Wiley-VCH.

increasing the S loading (**Figure 10**). The authors synthesized the nanoscale sulfur@N-modified graphene oxide (S@EGO) wrapped structures by electrostatic adsorption. The graphene oxide was decorated with ethylenediamine (EDA), which reduced the sulfur core during recrystallization. Wrapped particles have a size of 3 × 5 mm, which includes a size of 20 × 50 nm for the nano-sulfur particles. The thermogravimetric analysis demonstrated that the material prepared through this method contained 92 wt% sulfur. The N-doped GO (EGO) exhibits a perfect wrapped state and catalytic activity at 85 °C, which is conducive to superior battery performance: discharge-specific capacity decreased from 1010 to 440 mAh g^{-1} (900 cycles at 1 C) with a decay rate of 0.0627%.

Han et al.[83] developed a 3D porous structure based on point-line-plane interfaces for LiSBs using CoSe-CNF-GO-MXene (CCGM) as a free-standing CoSe-CNF-GO-MXene (CCGM) sulfur host. A combination of two-dimensional (2D) graphene, MXene, and one-dimensional (1D) nanocellulose fibers with zero-dimensional (0D) transition metal selenide (CoSe) demonstrates good electrical conductivity and enhanced catalytic performance. Moreover, with a rationally designed porous structure (from 0D to 3D), ion and electron transport channels are well connected, contributing to good kinetic performance. A CoSe catalytic material with moderate adsorption energies has been demonstrated to be capable of catalyzing both precipitation and dissolution of Li_2S, enhancing the kinetics of the conversion process. A synergistic effect of CoSe, $Ti_3C_2T_x$, and graphene was demonstrated using density functional theory (DFT). The S@CCGM cathodes exhibit a high initial discharge capacity of 1205.1 mAh g^{-1} at 0.2 C and good long-term cycling performance. As a result, the gel electrolyte Li-S pouch cell passes all three tests: the 0–180° bending test, the nailing test, and the cutting test. With such a design, electrochemical energy storage devices can be made safe and flexible. **Table 2** summarizes recent key works on improved LiSBs with high specific capacity, enhanced rate performances, and increased charge–discharge cycles based on graphene oxide-based nanocomposites for sulfur cathode preparation.

4. Reduced Graphene Oxide (rGO) Based Composites as Sulfur Hosts

This section critically summarizes various rGO-based nanocomposites as potential host materials for high-performance LiSBs. Saroha et al. developed porous microspheres comprised of reduced graphene oxide-carbon nanotube (rGO-CNT) frameworks with well-embedded cobalt selenide nanocrystals coated with N-doped graphitic carbon (NGC), which were used to enhance the performance of LiSBs (**Figure 11**).[89] Decomposed PS nanobeads form macropores that efficiently penetrate electrolytes and ensure short diffusion paths. Furthermore, the CoSe2 nanocrystals provide a multitude of polar active sites that effectively anchor polysulfide intermediates, reducing material loss. With nanostructure merits, Li-S cells utilizing a P–$CoSe_2$@NGC/rGO–CNT-coated separator and a conventional sulfur electrode demonstrated outstanding rate capability (up to 2.0 C) and remarkable cycling stability (1000 cycles at 2.0 C).

In a recent study, Suriyakumar et al.[90] reported a method for restricting polysulfide crossover and enhancing elemental sulfur conductivity. Cathodes are prepared from the Fe_3O_4-seated rGO–sulfur complex (**Figure 12**). The LiSB delivers a discharge capacity of 1400 mAh g^{-1} at 0.1 C-rate on its first cycle, whereas 0.5 C-rate achieves a steady discharge capacity. Each element of the composite

Table 1. Summary of graphene-based composite materials as potential sulfur hosts.

Material	Description	Specific capacity (mAh g^{-1})	Number of cycles	Capacity retention (%)	Reference
Monodisperse sulfur nanoreactors on graphene	A chip-inspired design of a vertically integrated structure as an LSB cathode by implanting Mo_2C nanoparticles and nanosulfur into the graphene matrix. This configuration enabled the synthesis of isolated sulfur nanoreactors (S-NRs) integrated into a tandem array, generating chip-like integrated LiSBs. The spatial confinement/protection and concentration gradient of the S-NRs effectively avoided the dissolution, diffusion, and loss of polysulfides, thereby enhancing the sulfur utilization and redox reaction kinetics. The adaptive storage energy can be improved by utilizing the tandem, isolation, and synergistic multiplicative effect among the nanoreactor units.	1392 at 0.1 C	1500	A low-capacity decay rate of 0.017% at 0.5 C	[38]
Flexible lithium-sulfur battery cathodes made of phosphorus-sulfur/graphene composites	Through a one-step PS additive reaction at 320 °C, PS/G composite cathodes achieve high volumetric capacities with high sulfur packing densities. PS/G composites are self-supporting, bendable, and compressible and can easily be made into a binder-free LiS cathode sheet. Their cathode sulfur density is 1.8 g per cubic centimeter (80% active materials content).	The specific capacity is 959 mAh g^{-1}, and the areal capacity is 5.5 mAh cm^{-2}	200	Low capacity fading within 200 cycles (~60% utilization)	[39]
Sulfurized-polyacrylonitrile/graphene (2D-SPAN/G) cathode	A compact, high-performance, 2D sulfurized-polyacrylonitrile/graphene (2D-SPAN/G) cathode for practical LiSBs. A 2D-SPAN/G cathode with a high active-mass (sulfur) loading of 10 mg cm^2 g^{-1} is successfully prepared *via* high-pressure pelletization. In the 2D-SPAN/G cathode, graphene nanosheets function as a robust and conductive scaffold, which uniformly encapsulates SPAN nanoparticles, providing structural integrity and enabling the high electrochemical utilization of sulfur.	A high areal capacity of 11 mAh cm^{-2}	300 cycles at a high current density of 4 mA cm^{-2}	—	[43]
VO_2 nanotube/graphene binary sulfur host	A VO_2/G binary sulfur host is constructed by combining VO_2 nanotubes with graphene (G), which have a relatively higher redox potential than sulfur. By chemically adsorbing soluble LiPSs in such an environment, VO_2 nanotubes can optimize the electrochemical conversion kinetics of LiPSs, inhibiting the shuttle effect.	1050 at 0.2 C	500	541 mAh g^{-1} after 500 cycles at 2.0 C	[40]
$MoTe_2$@graphene composites	$MoTe_2$ nanosheets were grown on highly conductive graphene support through a simple and ultrafast microwave-assisted chemical coupling and heating method to develop hybrid sulfur host materials. $MoTe_2$, with superb electrocatalytic activity, forms a nano reservoir that contains elemental sulfur, intermediate LiPS species, discharge product Li_2S, and accelerates electron transfer.	1246 mAh g^{-1} at 0.2 C	100	98.7% capacity retention after 100 cycles at 0.2 C	[37]
Mesoporous carbon-sulfur with graphene-nitrogen-phosphorus-fluorine (G-NPFMC-S) doped with nitrogen, phosphorus, and fluorine (N)	These promising results can be attributed to the structure formed inside the G-NPFMC-S film, as that highly porous NPFMC can provide adequate storage space for sulfur loading. In addition, the insertion of the graphene network and the N, P, and F-doped carbonic interface hinders the LiPS shuttle via chemical adsorption and a physical barrier.	1356 at 0.1 C	500	A capacity decline rate was 0.025% per cycle	[44]
Holey graphene/ferroelectric/sulfur composite (S/FNPs/hG)	Composite sulfur/ferroelectric nanoparticles/holy graphene cathodes (S/FNPs/hG) were developed for high-mass-loading S cathodes. Holey graphene, a unique dry-pressable electrode for LiSBs, enables solvent- and binder-free procedures. Graphene's holey structure facilitates fast electron and ion transport, affording enough space to mitigate the electrode's volume expansion. As a result of ferroelectric polarization in S/hG composites, an internal electric field is generated, reducing the unwanted shuttling effect.	1409	18	90	[45]

Table 1. Continued

Material	Description	Specific capacity (mAh g^{-1})	Number of cycles	Capacity retention (%)	Reference
FeCoNG material comprises Fe and Co dual-atom moieties anchored to N-doped multilayer graphene	Based on theoretical calculations, it was determined that the Fe–N_4 moiety binds stronger to low-order LiPSs than the Co–N_4 moiety does to high-order lithium polysulfides. FeCoNG outperforms NG due to its efficient catalytic conversion of soluble lithium polysulfides into solid lithium sulfides. This study confirms that in LiSBs, single-atom catalysts have a high catalytic efficiency.	878.7 at 0.2 C	100	77.4	[46]
Co_9S_8/CNTs-G	Polar Co_9S_8 encapsulated in pyrrole-modified graphene is prepared via pyrolysis. CNTs planted on Co_9S_8 nanoparticles (Co_9S_8/CNTs-G) are in situ formed. Co_9S_8/CNTs-G bears high sulfur loading and accelerates rapid electron transfer.	950 at 1 C	600	A decay rate of only 0.01% per cycle	[47]
Graphene modified with glutarimide/S	A polar organic molecule glutarimide (GIM) onto the nonpolar graphene (G) forms a G–GIM composite as host materials to accommodate sulfur and thus assemble the S/G–GIM cathode. First-principle calculations show that GIM can absorb G via the charge-transfer effect among its N atom and C=O double bond, while the latter can effectively anchor the otherwise dissolved lithium polysulfides to bring them into closer contact with G. Such a configuration is also validated by experimental measurements. Electrochemical tests on the S/G–GIM cathode exhibit high discharge capacity, better rate performance, and longer cycling stability compared to the S/G cathode without GIM.	1327 at 0.2 C	500	—	[48]
Nickel (Ni) single atoms and clusters anchored to a porous hydrogen-substituted graphdiyne support (termed Ni@HGDY), which is incorporated in Li_2S cathodes.	The rapidly synthesized catalyst decreased the reaction overpotential and promoted a complete conversion between Li_2S and sulfur.	516 at 1 C	125	—	[49]
3D Holey graphene/polyacrylonitrile sulfur composite (3D-HG/PAN/S)	A 3D-HG/PAN/S cathode for LiSB has been developed. Due to its unique architectural design, the 3D HG framework ensures fast electron and ion transport inside the thick electrode. This provides enough space for the electrode to expand without expanding too much.	—	1500	An ultra-low capacity decline rate of 0.012% per cycle	[50]
MoS_2 and graphene	Using N-doped graphene and carbonized melamine foam based on theoretical calculations, a multifunctional coating layer for LiSB is designed and constructed. MoS_2 and nitrogen-doped carbon composite with Mo–O–C bonds can catalyze polysulfides with Gibbs free energies of 0.19 eV and dissociation energy barriers of 0.48 eV owing to a strong covalent coupling effect.	1274 at 0.2 C	1000	The self-discharge rate was 8.6% after 5 days at 0.5 C	[51]
VSe_2/G/CC/S	An ultra-high-performance sulfur host made from vanadium diselenide (VSe_2) and vertical graphene on carbon cloth (CC)	A high specific capacity of 4.9 mAh cm^{-2} with a high sulfur loading of 9.6 mg cm^2 g^{-1}	800	An ultra-low capacity decline rate 0.039% per cycle	[52]
G/S	Developing a graphene-sulfur cathode with very high sulfur loading, whereby the sulfur chains are immobilized by covalent bonding to graphene. The loading in covalent-sulfur reached an unprecedented 80 mass%, increasing the full-cell specific capacity and, importantly, limiting the shuttling effect even at very low specific currents, thus ascribing outstanding cycling stability.	700 at 0.1 C	500	—	[53]

Table 1. Continued

Material	Description	Specific capacity (mAh g^{-1})	Number of cycles	Capacity retention (%)	Reference
Sandwich-structured G@CoS@Carbon Fiber/S	The exposed interfaces effectively decrease Li_2S decomposition by releasing Li^+ onto the circumjacent graphene surface with a low Li^+ diffusion barrier and anchoring the remaining Li-S bond on the exposed CoS interface with a high adsorption energy. The unique structure consists of catalytic CoS nanosheets and defective RG coating. As a result of the interwoven fiber interlayers, only the Li^+ diffusion can be coupled with the electron transfer, and the polysulfide reaction can be efficiently regulated, enabling both LiPS conversion and Li_2S decomposition to occur synergistically.	629 at 2 C	420	—	[54]
Metallic MoS_2 nanoflowers decorated graphene nanosheet/S	FM@G comprises sulfur-deficient metallic 1T-MoS2 nanoflowers onto with graphene (SulM@G), which are systematically modified on the separator as well as the cathode.	A high specific capacity of 1360 under a sulfur loading of 5.1 mg cm^2 g^{-1}	500	71.7	[55]
Sulfonated-graphene@sulfur nanocage	This paper describes a facile template-free self-caging nanotechnology for creating graphene@sulfur nanocages. This is accomplished by developing a new sulfur-graphene nanochemistry based on reductive sulfur solutions and oxidative sulfonated graphene dispersions. Sulfonated graphene nanocages are successfully synthesized in situ by mechanical mixing and embedded into reaction-induced self-assembled sulfur particles. By combining strong chemical absorption and physical blocking, these nanocages not only accommodate the large volume changes in active materials but also exhibit strong polysulfide trapping capabilities.	—	2000	A low capacity decline rate of 0.019% per cycle at 0.5 C	[56]
Nitrogen-doped graphene decorated with vanadium nitride nanoparticles (VN/NG)/S	The electrochemical results demonstrated that the VN/NG could trap the LiPSs, guide the rapid deposition of insoluble Li2S in the discharge process, and improve the oxidation kinetics of Li_2S during the charging process. The catalytic effects of VN/NG towards both directions of redox are verified by the calculated activation energy (E_a), which is smaller than the counterpart with separators modified by nitrogen-doped graphene (NG) substrate.	791 at 5 C	300	A low decaying rate of 0.068% per loop at 1 C	[57]
Vanadium nitride quantum dots/holey graphene (VNQD/HG/S)	This paper describes a facile approach to synthesizing nanostructured VN quantum dots (VNQDs)/holey graphene matrix that will stabilize the sulfur cathode by simultaneously promoting the trapping, anchoring, and catalyzing efficiencies of both LiPSs and Li_2S. Due to its abundant edge catalytic sites, graphene nanopores in-plane, and high electrical conductivity, the sulfur host not only adsorbs soluble polysulfides well, anchors solid Li2S well, and its rapid conversion kinetics are fast, but also provides abundant sulfur storage sites and efficient transport pathways for lithium ions and electrons.	1320	500	99.95	[58]
Nitrogen-doped graphene aerogel encapsulating sulfur.	A simple one-step hydrothermal method has been applied to design nitrogen-doped graphene aerogel (N-GA) with three nitrogen sources. Subsequently, sulfur was encapsulated in N-GA using a chemical deposition method to synthesize sulfur encapsulated in N-GA (N-GA/S) composites.	723.9	100 cycles at 0.7 C	87.4	[59]
Graphene quantum dots/sulfur (GQDs/S) composite	Multiple polar functional groups in GQDs can provide more active absorption sites to significantly strengthen the chemical absorption with polysulfides, suppressing the 'shuttle effect.' A highly dispersed GQD particle in the solution serves as a nucleation site; the sulfur dissolved in the solution is reprecipitated around the GQDs, forming a dendritic interlaced network structure that prevents sulfur from aggregating and enhances active substance absorption.	1125 at 0.1 C	100 cycles at 0.2 C	—	[60]

Table 1. Continued

Material	Description	Specific capacity (mAh g^{-1})	Number of cycles	Capacity retention (%)	Reference
Sulfur-doped graphene nanofiber network	Chemical vapor deposition (CVD) and ball milling can effectively incorporate sulfur into a 3D nanofiber network of high-quality graphene. As a result of the high-quality graphene network, Li^+ and electrons could be transported efficiently in continuous and durable channels. Also, in-situ sulfur doping permits desirable interactions with the entire sulfur species, preventing sulfur loss and facilitating sulfur redox reactions.	Using 15 mg cm^2 g^{-1} of sulfur exhibits a high reversible areal capacity of 13.1 mAh cm^{-2}	300 cycles at 0.5 C	—	[61]
3D hierarchical graphitic carbon foam supported graphene@Mo_2C (GCF-G@Mo_2C)	The N-doped carbon foam wrapped by graphene sheets with an agaric-like porous structure could promote fast electron and ion transport, meanwhile effectively anchoring the polysulfides through physical confinement and chemical adsorption by strongly polar-polar interactions. More importantly, the Mo_2C can act as the chemical anchoring center to provide strong polysulfide adsorption, as testified by experimental data and first-principle calculations. Moreover, the catalytic effect of Mo_2C also accelerates the redox kinetics of polysulfide conversion.	862 mAh cm^{-2}	500	0.051% capacity fade per cycle at 1 C rate	[62]
N, P co-doped graphene modified with phosphorus-Fe_4N/S	It was synthesized by using a simple solvothermal method, followed by the co-doping of nitrogen and phosphorus in graphene nanosheets (P-Fe4N@NPG), which were then used as sulfur hosts in lithium-sulfur batteries after nitriding and phosphating calcination. P-Fe4N@NPG/S cathode exhibits excellent electrochemical performance due to multiple compositions, and unique structure	1386.1 at 0.1 C (an outstanding areal capacity of 6.03 mAh cm^{-2})	417.4 mAh g^{-1} at 1 C after 1000 cycles	—	[63]
Three-dimensional conductive sponge framework using sulfonated carbon nanotubes/graphene	A 3D electrode made from graphene, carbon nanotubes, and sulfonated nickel foam. Nickel foam is woven with 1D multi-wall carbon nanotubes (MWCNTs) and 2D graphene (NG/CNTs) to form a continuously ion-electronic conductive 3D network. By forming ion-electronic conductive 3D networks, these materials enhance sulfur redox reaction kinetics. When the cathode surfaces are negatively charged, they become hydrophilic. In this way, it suppresses polysulfide shuttle effects and promotes polysulfide conversion by anchoring polysulfides with strong adsorption sites. A negatively charged group grafted onto lithium-ion speeds up lithium-ion transport fivefold.	1380 at 0.2 C	100	A capacity decay of 0.031% at 2 C	[64]
N-doped graphene composite/titanium nitride nanocrystals ((NG)/TiN)/S	Graphene sheets decorated with nanoparticles of TiN catalyze LiPSx electrochemical reduction and oxidation during discharge and charging. As a result of these two effects, the LiPSx dissolution is slowed, and the electrochemical reaction is accelerated, thus alleviating the shuttle effect.	1390 mAh g^{-1} at 0.1 C	300	—	[65]
Graphene scaffolds anchored on hierarchical CoP nanoflakes derived from MOF	Hybrid sulfur host developed from flexible carbon cloth (CC), vertically grown graphene nanoflakes over CC (G/CC), and metal–metal–organic framework-derived CoP anchored on vertical graphene (CoP@G/CC).	930.1 at 3.0 (a high areal capacity of 8.81 mAh cm^{-2} at 0.05 C)	500 cycles at 2.0 C	A low capacity fading rate of 0.03% per cycle	[66]
Phosphorus (P)-doped graphene (G)/carbon nanofiber (CNF)/sulfur (S) aerogel (PGCNF/S)	It has been demonstrated that hierarchical PGCNF/S with a "network" morphology can be used to wrap sulfur spheres in graphene sheets and carbon nanofibers (PGCNFs) with net structures. This carbon matrix improved the electrochemical performance of the sulfur sphere considerably. Using PGCNF nets, sulfur spheres are loaded uniformly, resulting in an 85 wt% sulfur mass loading. Additionally, the porous structure achieved with this PGCNF/S cathode can allow active sulfur spheres to expand sufficiently.	1360 at 0.1 C	600	—	[67]

Table 1. Continued

Material	Description	Specific capacity (mAh g^{-1})	Number of cycles	Capacity retention (%)	Reference
3D hierarchical graphene/CNT microspheres with nitrogen doping (3D-NG/CNTs/S)	3D-GCNT microspheres with perfect N-doping as potential sulfur hosts. This material retains the structural properties of 1D CNTs and 2D graphene and prevents polysulfide dissolution.	1465.1 at 0.1 C	500	—	[68]
Holey graphene modified $LiFePO_4$ hollow microsphere/S (HG-$LiFePO_4$/S)	$LiFePO_4$ (LFP) hollow microspheres are compounded with holey graphene (HG) through an electrostatic attraction strategy coupled with high-temperature treatment, resulting in HG/LFP binary hosts, in which LFP microspheres with relatively high redox potentials are essential for adsorption of lithium polysulfide intermediates. Facilitating the transition between long-chain LiPSs and short-chain Li_2S_2/Li_2S effectively suppresses the "shuttle effect" during charge and discharge.	1507 at 0.1 C (an ultrahigh areal capacity of 11.9 mAh cm^{-2} (0.1 C))	500	—	[69]
3D-interconnected nanoporous graphene (NPG) micro/nano-foams/S	3D-NPG micro-foams and nanofoams are developed via a new approach to solid-state catalytic growth. Both NPG microfoam and nanofoam exhibit similar nanoporous structures containing close tubular and open non-tubular pores but with different particle sizes. As electrochemical reactors for sulfur cathodes, sulfur is encapsulated inside the tubular pores. It was found that NPG nanoreactors can enhance electrochemical performances compared to NPG microreactors, including improved reversible capacities, cyclic performances, and rate performances.	1143 at 0.1 C	300	The capacity decay is only 0.15% per cycle	[70]
A highly N-doped carbon/graphene/ sheet (NC/G) is used to host sulfur	By combining abundant N active sites with high electrical conductivity, NC/G can anchor and convert LiPSs in situ. Both experimental investigations and theoretical studies demonstrate that such a host binds strongly to LiPSs and promotes redox kinetics.	1380	500	A low capacity decline rate of 0.037% per cycle	[71]
Sulfur-loaded Zr-based MOF-808 with graphene/ethyl cellulose as the active material.	Electrochemical results indicate that the nanocomposites deliver enhanced specific capacity over conventional carbon/binder mixtures, and molecular attachment with lithium thiophosphate further enhances the MOF's performance. The dense form factor of the sulfur-loaded MOF-graphene nanocomposite electrodes increases their volumetric capacity compared to other works containing much higher levels of carbon.	688	100	79.8	[72]
HG anchoring of the monodispersed nano-sulfur with covalently-grafted PAN	A novel "egg tray" hierarchical architecture of confining and uniformly distributing nano-sulfur into a 3D-HG framework with PANI crosslinking (3DHG/NS/CPANI) via photo-assisted method was designed for high-mass-loading cathode. HG contains both conductive skeletons as electron transfer paths and abundant void spaces in favor of homogenous sulfur anchoring. This configuration improves the contact between nano-sulfur and graphene for effective charge transportation and provides buffering space for volume variations during electrochemical processes.	1082 at 0.5 C	500	An ultra-low capacity decay of 0.04% per cycle over 500 cycles at 1 C	[73]
Nitrogen-doped porous carbon fiber (NF)/vertical graphene (VG)	A freestanding sulfur cathode based on NF@VG composites. The porous structure and nitrogen doping effectively enhance the absorption of polysulfides through physical confinement and chemical action, while the vertical graphene network significantly promotes electron transfer and boosts the catalytic conversion kinetics of polysulfides.	738 at 1 C	600	0.029% capacity fading per cycle at 1 C rate at a sulfur loading of 7 mg cm^2 g^{-1}	[74]

Table 1. Continued

Material	Description	Specific capacity (mAh g^{-1})	Number of cycles	Capacity retention (%)	Reference
Roller-like spore carbon sphere-orientated graphene fibers	Free-standing graphene fiber electrodes containing roller-like orientated spore carbon spheres via rheological engineering. With the help of the orientated microfluidic cospinning technology and the plasma reduction method, spore carbon spheres are self-assembled and orientedly dispersed into numerous graphene flakes, forming graphene fiber electrodes enriched with internal rolling woven structures, which cannot only enhance the electrical contact between active materials but also effectively improve the mechanical strength and structure stability of graphene fiber electrodes. When the designed graphene fibers are combined with the active sulfur cathode and lithium metal anode, the assembled flexible lithium-sulfur batteries possess superior electrochemical performance with high capacity, excellent cycling life, and good mechanical properties.	1000	—	—	[75]
N, S-doped graphene based on graphene oxide and thiourea-formaldehyde resin	Graphene and thiourea-formaldehyde resin are self-assembled in situ and calcined to synthesize nitrogen and sulfur-doped graphenes. Graphene doped with N, S serves as a conductive agent and a chemosorbent, preventing Li metal from corrosion and suppressing polysulfide shuttling to maximize reversibility and cycle life.	A specific capacity of 622 mAh g^{-1}	500	A low capacity fading rate of 0.049% per cycle over 500 cycles at 1 C	[76]
Co_9S_{8-x}/N-doped graphene (Co_9S_{8-x}/N-G)	The Co_9S_{8-x}/N-doped graphene allows the generation of sulfur vacancies by hydrogen reduction of stoichiometric Co_9S_8, and hence serves as a sulfur host material and electrocatalyst.	A high areal capacity of 12.9 mAh cm^{-2} under a high sulfur loading of 14.6 mg cm^2 g^{-1}	1000	A low capacity fading rate of 0.035% per cycle	[77]
Ferroelectric doped holey graphene/sulfur composite	This study reports the impact of the incorporation of ferroelectric nanoparticles (FNPs), such as $BaTiO_3$ (BTO), $BiFeO_3$ (BFO), $Bi_4NdTi_3Fe_{0.7}Ni_{0.3}O_{15}$ (BNTFN), and $Bi_4NdTi_3Fe_{0.5}Co_{0.5}O_{15}$ (BNTFC), as well as the mass loading of sulfur to fabricated solvent-free sulfur/holey graphene-carbon black/polyvinylidene fluoride (S/FNPs/CBhG/PVDF) composite electrodes to achieve high areal capacity for lithium-sulfur (Li-S) batteries. The dry-press method was adopted to fabricate composite cathodes. The HG, a conductive and lightweight scaffold derived from graphene, served as a matrix to host sulfur and FNPs for the fabrication of solvent-free composites.	1486 at 1 C	100	High	[78]
Polyaniline-modified waste-derived graphene/sulfur nanocomposite cathode	The authors reported, for the first time, the preparation of high-energy cathode materials from the nanocomposites (NCs) having polyaniline (PANI), waste-derived graphene (WDG) derived from plastic waste, and sulfur (S) for LiSBs.	880 at 0.1 C	160	400 at 160th cycle at 0.5 C	[79]

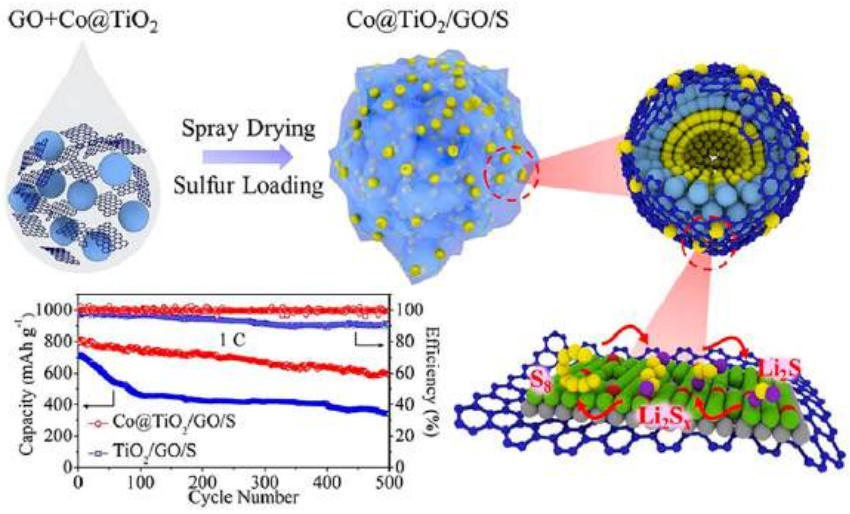

Figure 9. Lithium-sulfur batteries with cobalt-doped titanium dioxide hollow sphere clusters wrapped in graphene oxide.[80] Copyright 2021, Elsevier.

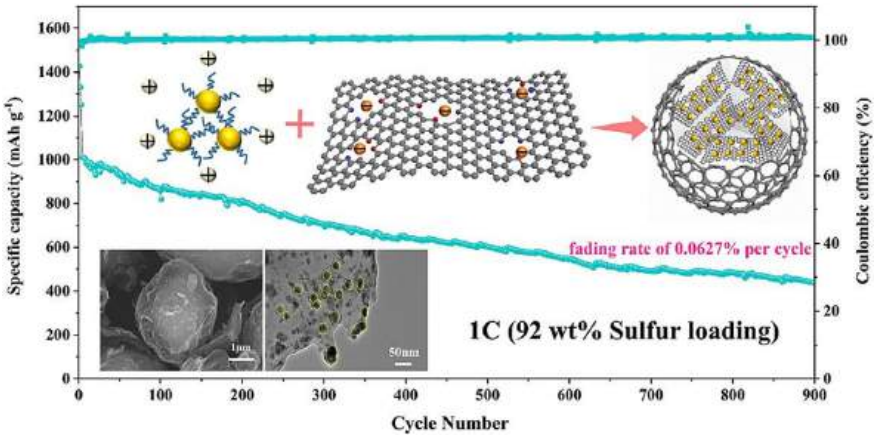

Figure 10. A graphene-wrapped nano-sulfur structure functionalized with ethylenediamine enhances LiSB's performance.[82] Copyright 2024, Elsevier.

cathode has a specific function: rGO enhances cathode conductivity, while Fe_3O_4 confines polysulfides appreciably, as shown by TEM and XPS analysis. In addition, self-discharge is reduced in the cell. Electrochemical impedance spectroscopy is used to systematically analyze variations in electrolyte resistance (R_s), interfacial resistance (R_i), and charge transfer resistance (R_{ct}) depending on the depth of discharge (DOD) and state of charge (SOC).

For the first time, Chen et al.[91] synthesized 3D-porous microspheres of nanosized sulfur particles, N-doped oxygen-deficient TiO_{2-x} nanorods, and reduced graphene oxide (N-TiO_{2-x}/rGO/S) as a potential sulfur host material using the spray-drying process (**Figure 13**). By incorporating void spaces in the microspheres, volumetric expansion is mitigated upon charge/discharge cycling, and sulfur utilization is improved. According to density functional theory (DFT) calculations, N-TiO_{2-x} nanorods enhanced the conductivity and exhibited strong capabilities for the adsorption and migration of lithium polysulfides. Consequently, the N-TiO_{2-x}/rGO/S cathode performed excellently at 1.0 C over 300 cycles with a specific capacity of about 700 mAh g^{-1}. Besides contributing to materials engineering and structural design, this novel design and preparation strategy improves the electrochemical performance of energy storage systems.

Using a combination of the Ostwald ripening process and hydrothermal treatment, Kim et al.[92] developed hierarchically structured MoO_2 nanoparticles with N, P-codoped reduced graphene oxide (N, P-rGO/h-MoO_2) (**Figure 14**). Afterward, hollow MoO_2 nanospheres were homogeneously distributed on rGO sheets. Through its hollow structure and volume buffering of sulfur, MoO_2 can act as a physical barrier to LiPS. Furthermore, N and P introduced with MoO_2 nanoparticles enhance sulfur immobilization and enhance LiPS redox kinetics. Cathode materials based on N, P-rGO/h-MoO_2@S demonstrated higher discharge capacity at 0.1 C and higher high-rate capacity at 10 C. Moreover, the N, P-rGO/h-MoO_2@S showed excellent long-term stability at 5 C and 10 C, with a low capacity decay rate of 0.043% and 0.029%, even after 900 cycles. It was found that N, P-rGO/h-MoO_2@S showed a high capacity of 5.0 mAh cm^{-2} with a high-capacity retention of 79.7% over 250 cycles.

Using two surface engineering strategies, Zhang et al.[93] demonstrate that a 2D-Ni-doped MoS_2/rGO composite can exhibit well-regulated surfaces and properties. Two distinct hydrothermal methods for doping nickel atoms into 2D MoS_2 nanosheets result in significantly different surface heteroatom content, as depicted in **Figure 15**. One method involves changing the valence state of surface heteroatom nickel with thermal reduction technology. Electrocatalytic activities of host materials can be significantly affected by the content and valence state of surface heteroatom nickel during the redox reaction processes of sulfur/Li_2S, thereby affecting the electrochemical performance of LiSBs. It is demonstrated that the S@3%Ni-MoS_2/rGO can be used as a sulfur host in lithium-sulfur cells and is capable of a high capacity. Through the rational regulation of the surface atomic structures and electronic states of sulfur hosts, this study can provide some inspiration for improving the electrochemical performance of advanced LiSBs.

Cyril Karima et al.[94] designed rGO-cobalt cathodes to facilitate polysulfide immobilization. Cobalt nanoparticles from the ZIF 67 metal–organic framework wrapped in rGO nanosheets increase the space inside the carbon sponge, thereby containing a substantial amount of sulfur (**Figure 16**). Due to its high affinity for lithium polysulfide, cobalt enabled robust lithium polysulfide adsorption against shuttling effects. The cobalt-carbon functional group bond prevents lithium polysulfides from dissolving in the electrolyte due to its bonding with the cobalt molecules. With sulfur and cobalt cohabiting on rGO, the electron transfer rate for sulfur transformation was accelerated,

Table 2. Summary of functionally modified graphene oxide (GO)-based composite materials as sulfur hosts.

Material	Description	Specific capacity (mAh g^{-1})	Number of cycles	Capacity retention (%)	Reference
Titanium dioxide hollow sphere clusters wrapped in graphene oxide and doped with cobalt as efficient sulfur hosts	A sulfur immobilizer with multi-level sulfur storage space consists of a cluster of Co@TiO_2 hollow spheres tightly wrapped by GO (labeled as Co@TiO_2/GO). This structure provided a multi-level sulfur storage space; the sulfur was encapsulated in the cavity of the Co@TiO_2 hollow spheres, between Co@TiO_2 spheres and GO sheets, and in the interlaminar pores of GO. This enabled the inner and outer surfaces of the Co@TiO_2 hollow spheres to participate better in lithium polysulfide (LPS) conversion reactions. Moreover, the incorporated Co NPs and abundant oxygen vacancies effectively captured LPS and boosted their redox reaction kinetics. Therefore, this multi-level sulfur storage space is very beneficial to the storage and blockade of polysulfides and the improvement of the energy storage performance of the LiSBs.	807 mAh g^{-1} at 1 C	500	A slow decay rate of 0.053% per cycle for 500 cycles	[80]
Hybrid polyaniline/graphene oxide/sulfur nanocomposite (PANI/GO/S)	The authors have developed PANI/GO/S nanocomposite in ice to grow continuous, well-ordered porous structures.	868 at 0.1 C	400	76	[81]
ZIF-67/S/GO	Zeolitic imidazolate framework, ZIF-S@GO-S (*n*) nanocomposites (*n* = 1, 2, and 3 for the mass ratio of ZIF-67/GO of 4:1, 6:1, and 8:1, respectively) as the cathode materials in Li-S batteries were successfully fabricated, and ZIF-S@GO-S (2) showed better electrochemical performances and cycle stability.	1529.5 at 0.1 C	500	High	[84]
GO@S/SFAC	This study designed and synthesized porous-layered GO@S/SFAC composites to solve the capacity fading problem of lithium-sulfur batteries caused by the shuttle effect. In the composites, the inner porous sisal fiber activated carbon (SFAC) provides a framework for accommodating active sulfur as a host; The outer GO restricts the dissolution and migration of polysulfides through physical confinement and chemical adsorption.	1364	100	—	[85]
Co_9S_8 nanotubes wrapped GO as potential sulfur hosts	A novel Co_9S_8@S/GO hybrid as host for the sulfur cathode. The GO and polar hollow Co_9S_8 nanotube can capture polysulfides in both physical and chemical adsorption.	1022 at 0.1 C	100	An ultralow fade rate of 0.027% per cycle at 1 C	[86]
Hollow mesoporous carbon spheres wrapped in GO as dynamic bipolar hosts	3D-GO wrapped hollow carbon spheres with straight mesoporous channels (termed "HMCS@GO") as a novel cathode host for LSBs with several integrated merits: 1) the hollow carbon spheres with a mesoporous shell afford a large interior void for the loading of sulfur species and serve as a conducting substrate for high utilization of the sulfur cathode with reduced polarization; 2) the wrapped graphene oxide layer with rich surface functional groups acts as a polar carrier for effective immobilization of soluble polysulfides and promotes their quick conversion during a charge/discharge process; 3) the hollow carbon spheres also effectively buffer the large volume fluctuation of the sulfur cathode during charge/discharge with enhanced structural integrity during long-term cycling.	—	—		
A self-supporting GO/CNT hybrid	A self-supporting (GO/CNTs) hybrid membrane for LiSBs was prepared using a facile vacuum filtration method. Lithium ions diffuse and transfer electrons quickly through CNTs. CNTs trap lithium polysulfides on GO sheets.	684.3 at 0.5 C	300	77.1	[87]
Covalent organic frameworks (COFs) wrapped by GO	A spray-drying process was used to synthesize GO-coated COFs. COF has polar groups that can efficiently adsorb LiPSs through lipophilic interactions, which reduces the shuttle effect caused by soluble LiPSs. A further benefit of using GO in the outer layer is that it can enclose discrete sulfur to reduce the loss of active substances, enhancing the cathode's cycle stability.	848.4 at 1 C	500	A low capacity decline rate of 0.058% per cycle	[88]

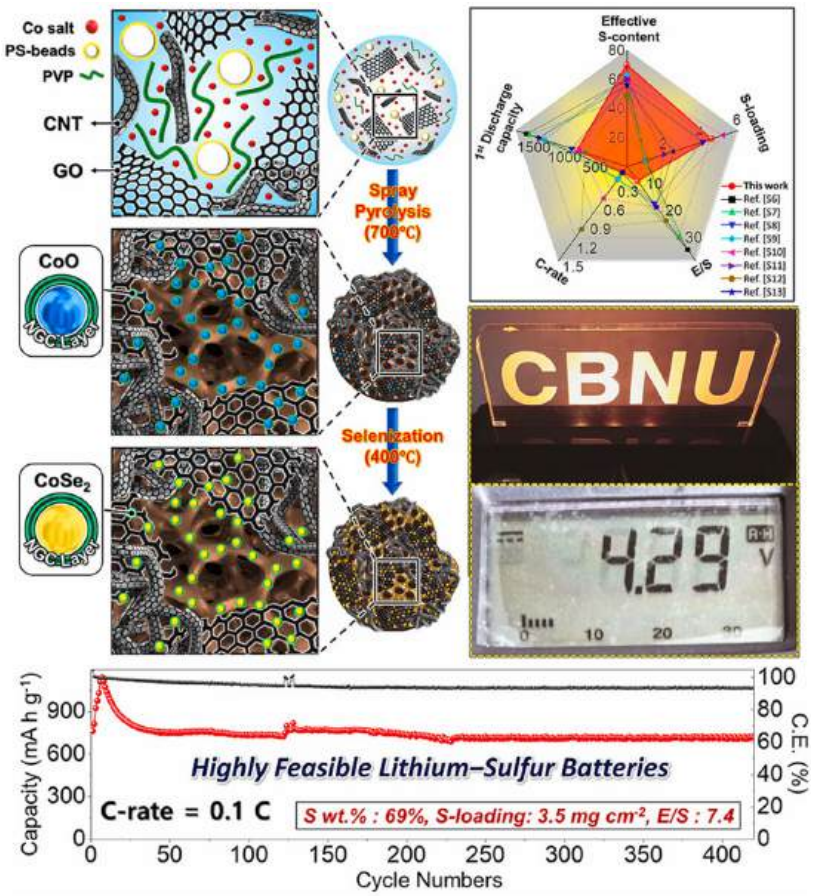

Figure 11. Integration of monodisperse sulfur nanoreactors on graphene to design high-performance LiSBs.[89] Copyright 2024, Elsevier

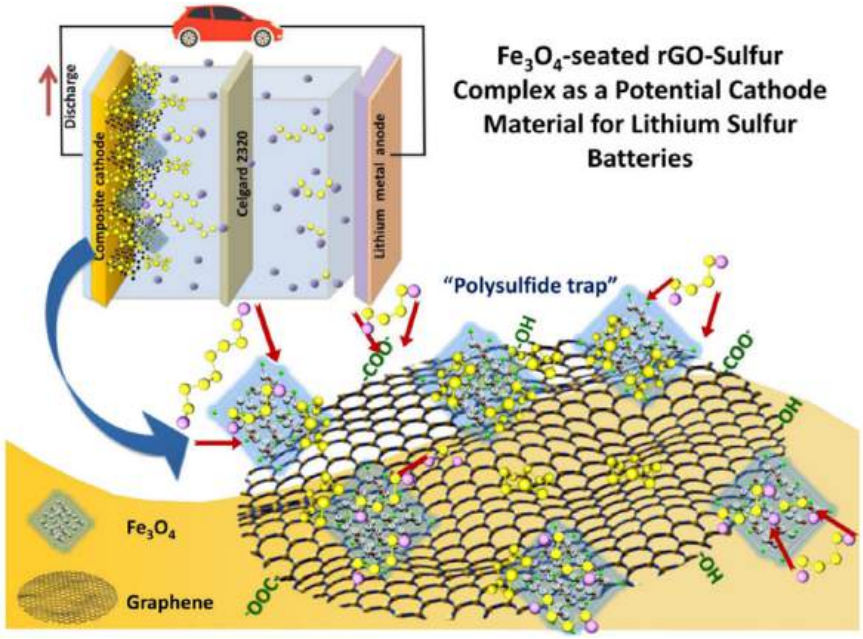

Figure 12. The role of Fe_3O_4@rGO in the ternary cathode for the Li-S cell.[90] Copyright 2020, Springer Nature.

resulting in efficient shuttle effect suppression and steady sulfur electrochemistry. Cobalt nanoparticles infiltrated into sponge sulfur show a discharge capacity of 1176 mAh g^{-1} at 200 mA g^{-1} current density with a 91% retention capacity for more than 140 cycles.

Deivendran et al.[95] described a system in which porous cobalt oxide nanocages (N–Co_3O_4) were embedded in a 2D graphene oxide nanoribbon (rGONR) carbon matrix, and a one-dimensional (1D) carbon nanotube (CNT) carbon matrix was used to form a double-shelled metal-carbon composite made of N–Co_3O_4/rGONR/CNT (**Figure 17**). Li_2S is incorporated into a porous nanocage carbon structure (N–Co_3O_4/C) using the infiltration-evaporation method. Its suitable pore size (2–14 nm) for polysulfides (PSs) confinement. The porous N–Co_3O_4 filler synergistically immobilized PSs via chemisorption, impeding the shuttle effect. This composite cathode has a high specific capacity at 0.1 C (1004 mAh g^{-1}) and on the 1000th cycle at 3 C (413 mAh g^{-1}), confirming good retention capability based on the as-fabricated Li_2S–N–Co_3O_4/rGONR/CNT. Hence, LiSBs offer promising applications in high-performance energy storage devices due to their excellent electrochemical performance with N–Co_3O_4/C-modified composite cathodes. **Table 3** summarizes recent key works on improved LiSBs with high specific capacity, enhanced rate performances, and increased charge–discharge cycles based on reduced graphene oxide-based nanocomposites for sulfur cathode preparation.

5. Summary and Outlook

This article comprehensively summarizes the potential applications of pure graphene, heteroatom-modified graphene, and graphene-based nanocomposite frameworks as potential hosts for sulfur to develop promising cathode materials for next-generation LiSBs. The aim is to develop LiSBs with high energy densities and extended cycle capabilities and promote their long-term application and development. The composite sulfur structure and graphene's simple framework support this viewpoint. Sulfur cathodes have been designed in various structures, such as sandwich, core-shell, and hybrid configurations. The electrochemical performance of LiSBs has improved rapidly due to graphene's flexibility and controllable assembly capabilities. In the field of graphene cathodes modified with heteroatoms, pyridinic-N proved to have greater chemisorption energy than other compounds.

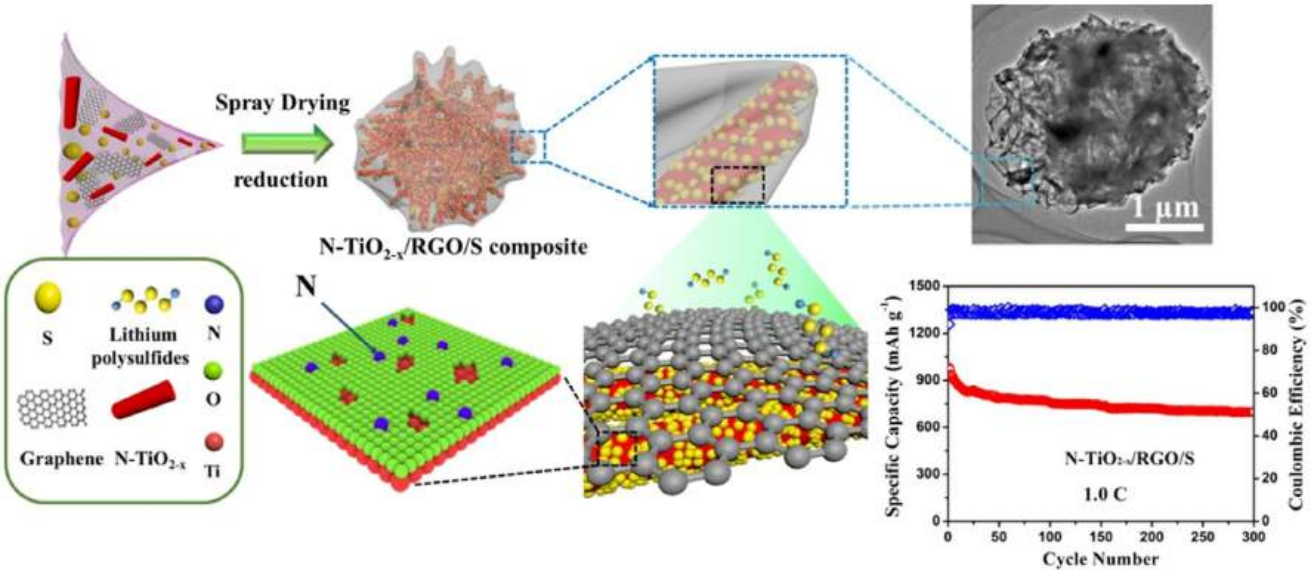

Figure 13. Schematic diagram of LiSB using N-TiO_{2-x}/RGO/S cathode.[91] Copyright 2019, Elsevier.

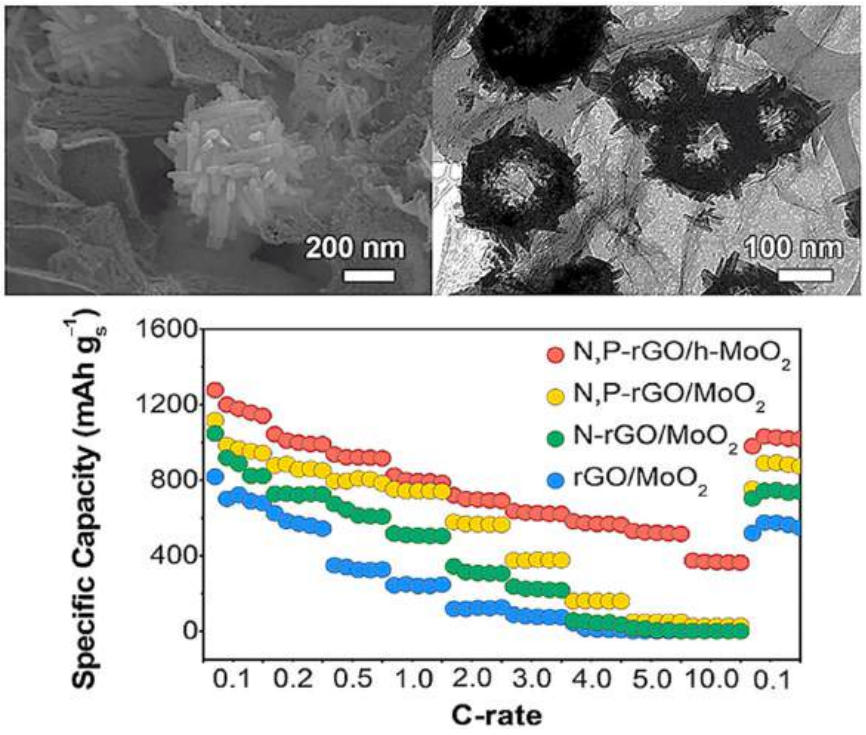

Figure 14. Hierarchically structured polyoxometalate-derived N, P-codoped rGO /MoO_2 composites for high-performance LiSBs.[92] Copyright 2023, Elsevier.

Doping transition metals exhibits additional electrocatalytic capabilities in addition to chemical bonding. Researchers have gradually developed a method of capturing LiPSs by various chemical bonds using diatomic-doped graphene to overcome the limited content of single-atom doping. In the S electrode, metal compound additives fix polysulfides and catalyze redox reactions to promote polysulfide conversion. A few metal compounds can also be used as active materials to store lithium, thereby increasing lithium storage capacity. By combining other carbon materials with graphene, we can reach a diversified conductive network structure, which enhances the conductivity of the skeleton, increases sulfur content, and expands pores.

Despite many attempts to improve the electrochemical performance of LiSBs, numerous challenges remain. For example, repeated experiments have confirmed pyridinic-N's stronger bonding force, but accurate control of the type and presence of nitrogen doping is impossible. In addition to the high cost, the complex doping process, and the lack of characterization accuracy, doping is challenging to carry out. It is still unclear how transition metal bonds interact with graphene bonds. Doping heteroatoms also presents many challenges. Despite adequate chemical bonding and catalytic conversion, metal additives do not have ideal conductivities, which inevitably reduces battery capacity and cycle capability. This may result in unexpected performance electrochemical results. Regarding chemical properties, graphene substrate materials act as a chemical bonding agent and catalyze electrochemical reactions. Dissolving polysulfides is key to improving the electrochemical performance of graphene substrate materials. Physical encapsulation and van der Waals forces should be studied mainly to inhibit polysulfide diffusion. Combining physical and chemical action is expected to be the most effective way to inhibit the LiPSs and the shuttle effect.

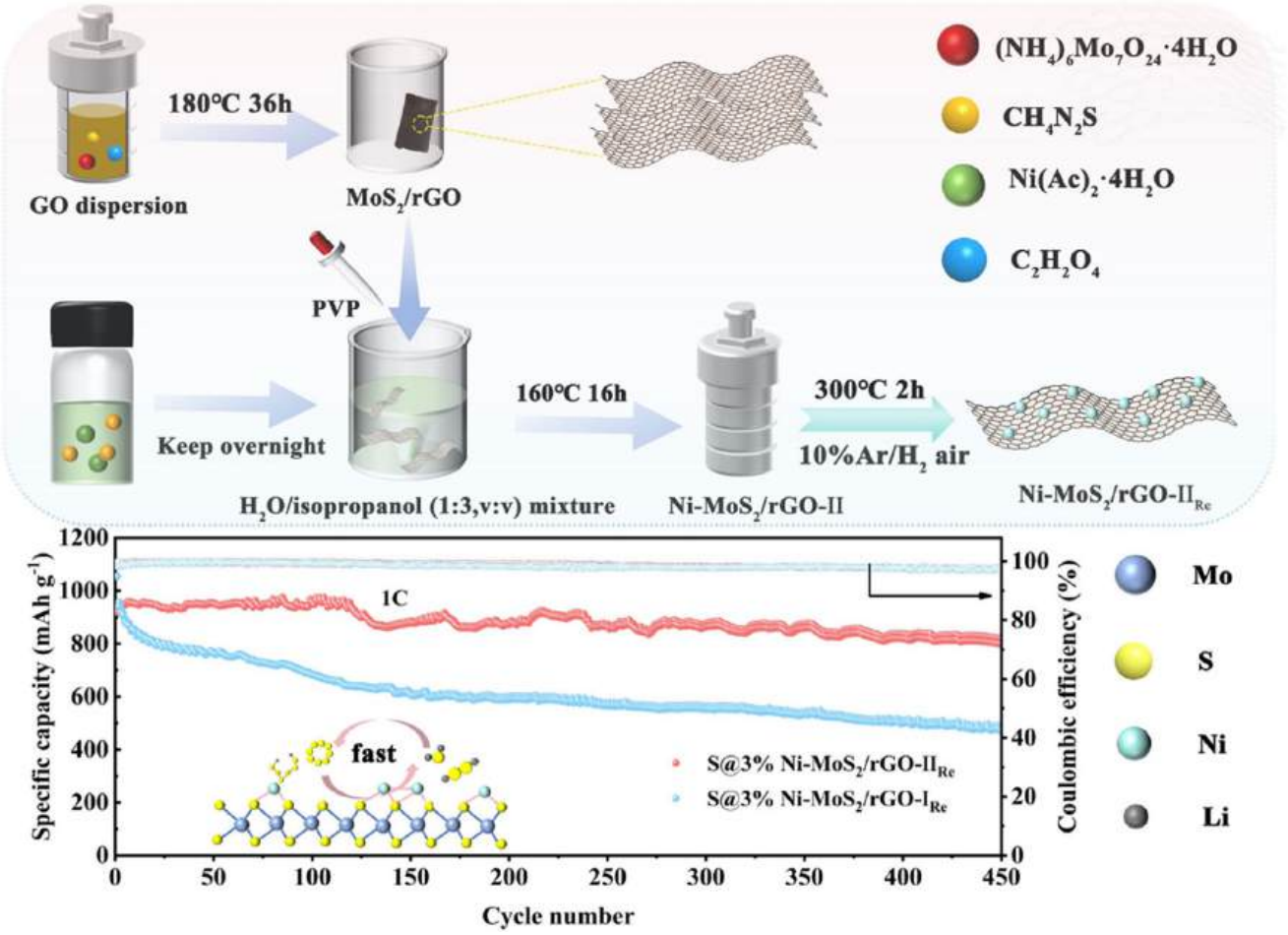

Figure 15. Heteroatom surface engineering with distinct doping ways and valence state regulation: Boosting electrocatalysis performance of Ni-doped MoS_2/rGO host for excellent lithium-sulfur batteries.[93] Copyright 2024, Elsevier.

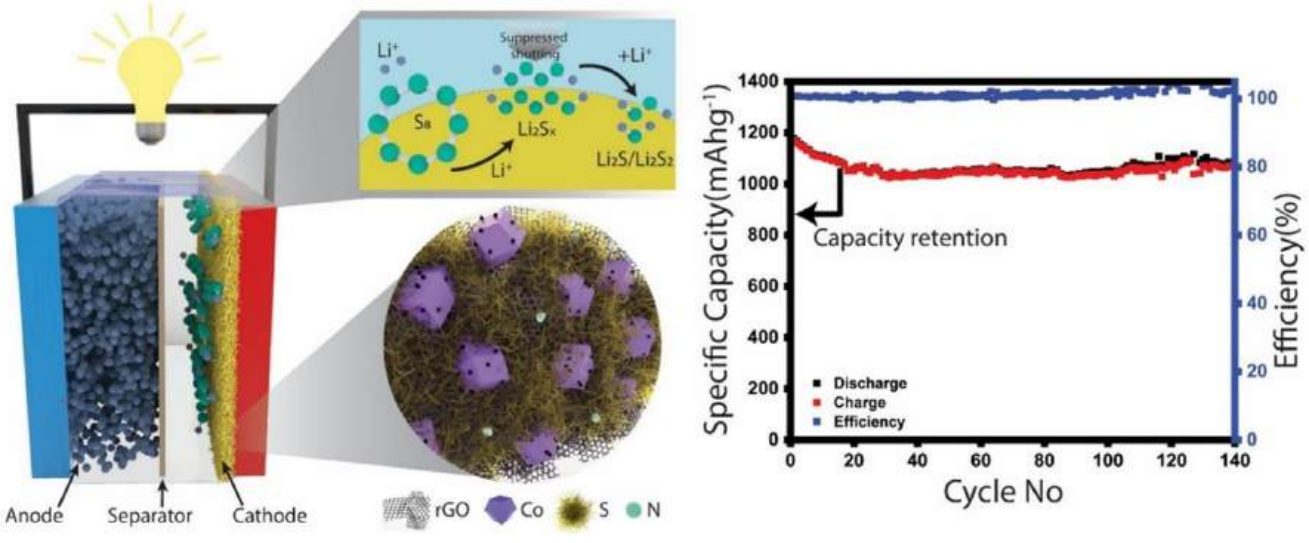

Figure 16. Interaction mechanism between MOF-derived cobalt/rGO composite and sulfur for long cycle life of lithium-sulfur batteries.[94] Copyright 2024, Elsevier.

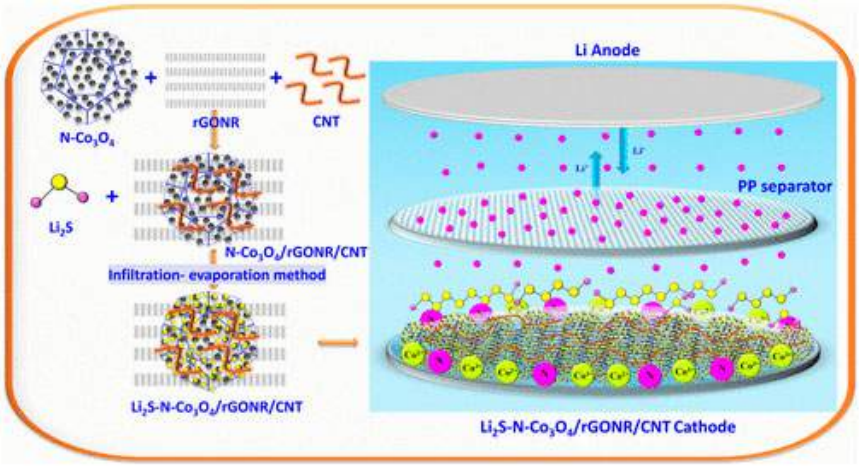

Figure 17. Study of fast catalytic conversion of polysulfides by porous N–Co_3O_4 nanocages embedded with rGONR/CNT composite for high-rate Li_2S-based lithium-sulfur batteries.[95] Copyright 2024, American Chemical Society.

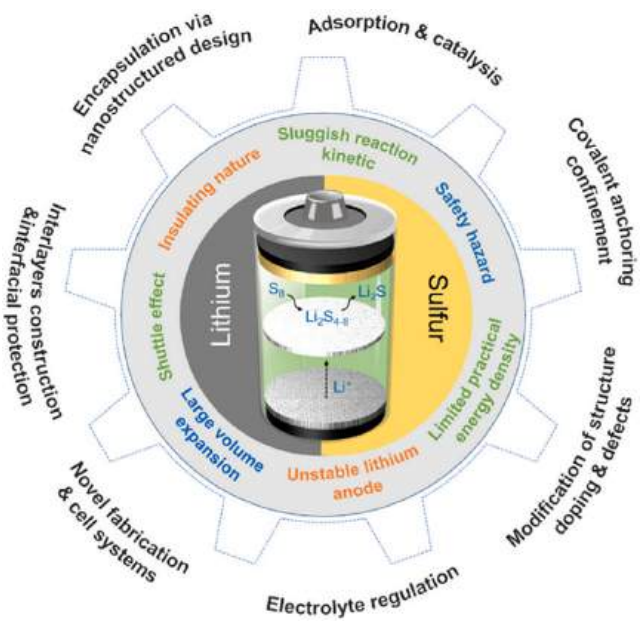

Figure 18. Current research and future development directions of LiSBs.[143] Copyright 2021, Elsevier.

To advance the commercialization of LiSBs, optimizing discharge capacity, long-term stability, rate performance, and other critical parameters is essential. Currently, the areal capacities (below 4 mAh cm^{-2}) often fall short of meeting the standards necessary for practical electrical devices, which typically require capacities exceeding 6 mAh cm^{-2}. To effectively compete with commercial Li-ion batteries, the primary focus should be on maintaining cycling stability and high-rate capability under conditions of high sulfur loading. A notable drawback of LiSBs is their lower volumetric energy density, which ranges from 550 to 600 Wh L^{-1}, particularly when compared to theoretical energy densities. Volumetric capacity is a critical metric closely associated with tap density, necessitating the use of lightweight yet compact electrode materials. Given that sulfur has a low intrinsic tap density (0.8 g cm^{-3}) and that porous hosts with large cavities result in poor packing, leading to excess space and increased surface area, minimizing the effects of porosity without compromising high gravimetric energy density is imperative. To achieve an optimal combination of high areal and volumetric capacity, it is essential to concentrate on the innovative utilization of advanced materials and structures. This approach aims to create a harmonious balance between maximizing the areal loading of sulfur and ensuring an appropriate tap density that meets performance requirements. By exploring new materials and structural designs, we can enhance the efficiency and effectiveness of energy storage solutions in this context.

There is still a long way to go before LiSBs can be manufactured industrially, and for the commercial application of LiSBs, coordination of development in many aspects is needed, including the preparation process, the applicable environment, the high energy density, and the economic benefits. A practical approach involves designing ordered, dense, nanostructured cathode materials requiring minimal quantities. For example, heavy transition metal oxides and their carbon composites could be strong candidates for enhancing tap density due to their higher density. Another potential strategy is to create an integrated cathode that eliminates the need for a binder or metal current collector, thereby improving volumetric performance. In conclusion, LiSBs are emerging as a promising candidate for the next generation of large-scale energy storage systems. While it is clear that it is not feasible to resolve all issues hindering the commercialization of LiSBs simultaneously, it is essential to review key strategies that offer in-depth insights into enhancing electrode performance, optimizing electrolytes, and improving overall cell design. This paper will guide future research aimed at making LiSBs a viable option. The current study and future development directions of LiSBs are summarized in **Figure 18**.

Table 3. Summary of reduced graphene oxide (rGO)-based composite materials as sulfur hosts.

Material	Description	Specific capacity (mAh g^{-1})	Number of cycles	Capacity retention (%)	Reference
Nitrogen-doped graphitic carbon-coated cobalt selenide nanocrystals within porous 3D graphene-carbon nanotube microspheres	Porous microspheres with a three-dimensional rGO–CNT framework are prepared. Comprising well-entangled N–doped graphitic carbon-coated $CoSe_2$ nanocrystals. $CoSe_2$ nanocrystals ensure efficient anchoring of LiPSs. The rGO-CNT framework improves the structural integrity and overall conductivity. P–$CoSe_2$@NGC/rGO–CNT interlayer exhibits improved electrochemical performance.	900 at 1.0 C	1000 cycles at 2.0 C	—	[89]
VO_2/rGO/S composites	The polysulfide can be anchored by the polar VO_2 plates. In addition, the conductive rGO network accommodates volume changes during cycling by providing electron transport channels.	493.4 at 0.5 C	700	High	[96]
CNT/rGO/S	The hierarchical structure of carbon nanotubes branched from anchored nickel nanoparticle seeds, and uniform distribution of sulfur is attributed to the sufficient space to impregnate sulfur, and the lithium polysulfides capturing sites.	829.3 at 0.5 C	200	High	[97]
Ascharite/rGO/S	In the ascharite/rGO aerogel hosts, the enhanced adsorption ability due to the formation of Mg-S and Li bonds, the rapid and continuous electron/ion transports, and the effective deposition of Li_2S are combined. Furthermore, the electrochemical results indicate that polarity matters for electrochemical performance of ascharite components for the S cathode.	850.5 at 1.0 C	500	High	[98]
MoS_2/rGO/CNTs/S	Composite MoS_2/rGO/CNTs with a three-dimensional (3D) network structure was constructed. The 3D porous skeleton composed of rGO and CNTs could act as a 3D conductive network, which not only significantly improved the conductivity and structural stability of the cathode material for LiSBs but also provided a large number of active sites for the active substance S. MoS_2 had a strong chemisorption effect on lithium polysulfides, which could effectively hinder their shuttle behavior.	1417.8 at 0.1 C	200	High (capacity decay rate per cycle was only 0.09%)	[99]
PVP/MoS_2/rGO/S	MoS_2 is grown in situ on graphene oxide flakes by a one-step hydrothermal method. Poly(vinyl pyrrolidone) (PVP) is added to modify the morphology of MoS_2, resulting in a 3D spherical layer structure. The spherical molybdenum disulfide can better adhere to graphene flakes, providing diffusion channels for lithium-ion transfer. Moreover, smaller particle size molybdenum disulfide forms more and stronger Mo–S bonds to anchor the polysulfide, thereby the cleavage of Li-S bonds of lithium polysulfide being promoted, and S–S bonds of sulfur to accelerate the electrochemical reaction.	789 at 1 C	200	—	[100]
S, N-doped rGO/Zinc sulfide (SN-rGO/ZnS)	A facile and solvent-free microwave synthesis for a composite material based on doped (sulfur and nitrogen) reduced graphene oxide embedded with zinc sulfide nanoparticles (SN-rGO/ZnS) to improve the battery performance. The SN-rGO/ZnS/S cathode showed a strong affinity towards polysulfides, thus reducing their loss by diffusion and improving redox kinetics, allowing for faster LiPSs conversion.	517–648 at 1 C	750	48.2	[101]
ZnCo LDH/rGO/S	A rGO-wrapped hollow ZnCo layered double hydroxide (ZnCo-LDH) microsphere is fabricated as sulfur host material. The rGO offers efficient charge transportation pathways. Meanwhile, the porous rGO and hollow ZnCo-LDH provide sufficient space for sulfur storage and mitigate the volume variation during battery charging and discharging. In addition, ZnCo-LDH exhibits excellent chemical adsorption capacity for polysulfides, and promotes their electrochemical conversion reactions.	1365.4 at 2 C	500	0.036% capacity decay per cycle	[102]
Polyaniline/rGO/S	The rGO provides a conducting carbon framework for improving the conductivity and mechanical stability of the cathode; polyaniline provides polar groups to restrain soluble lithium polysulfides (LiPS) by physisorption/chemisorption and separator modification with GO to act as a second barrier layer to suppress LiPS migration and support the cathode current collector to enhance sulfur utilization. The combination of these strategies led to an LiSB cell that exhibited high initial capacity, low-capacity fade, improved lithium-ion diffusion, and lowered cell impedance.	807 at 100 mA g^{-1}	500	Lower capacity fade of 0.02% per cycle	[103]
iPANI@rGO-CNTs/S	Iminated polyaniline (iPANI) is used to achieve energetic engineering to induce mid-energy level to the adsorption of polysulfides, and catalyze the redox conversion of sulfur species, and realize morphological engineering via self-assembly of iPANI onto a scaffold integrated by reduced graphene oxide (rGO) and carbon nanotubes (CNTs), namely iPANI@rGO-CNTs.	1144 at 0.5 C	300	71.3	[104]
S@rGO-rGO	The rGO sheets are introduced into a supersaturated sulfur solution, resulting in the uniform crystallization of sulfur on the rGO sheets. This process also effectively inhibits the shrinking and stacking of the rGO sheets. Thus, it is possible to adequately utilize sulfur during the charge/discharge process even when the sulfur mass ratio is high at 70%.	1669.1 at 0.1 C	400	76.87	[105]
S/FeMn PBA@rGO	3D microspheres composed of FeMn Prussian blue analog (FeMn PBA) and rGO were realized through spray drying technology. The FeMn PBA@rGO composite shows a distinctive microsphere structure with a wrinkled surface, in which rGO closely coats the FeMn PBA polyhedron. This unique structure with a well-coated shell could enhance structural stability and provide effective charge transfer channels at the cathode/electrolyte interface. Moreover, the polar FeMn PBA could provide abundant adsorptions to capture soluble LiPSs and catalytic sites to accelerate LiPSs conversion reaction effectively.	1145 at 0.2 C	Good cycling stability	—	[106]

Table 3. Continued

Material	Description	Specific capacity (mAh g^{-1})	Number of cycles	Capacity retention (%)	Reference
rGO/polycation/sulfur	The rGO/polycation/sulfur composites are promising cathode materials for Li-S battery applications because homogeneously dispersed sulfur nano/micro clusters in suitable carbon hosts enable remarkable cycle life for Li-S battery cells.	522 at 0.2 C	100	91.4	[107]
rGO/Ti_3C_2 QDs/S	A simple and scalable spray drying strategy was used to construct conductive polar Ti_3C_2 MXene quantum dots (QDs)-decorated reduced graphene oxide (rGO) microsphere (rGO@Ti_3C_2 QDs) as an efficient electrocatalyst and absorbent for Li-S battery. The Ti_3C_2 can effectively adsorb and catalyze LiPS conversion. This ability can be attributed to the Ti_3C_2 QDs providing many LiPSs catalytic active sites. In addition, the rGO provides physical LiPSs constraint and a flexible substrate to prevent QDs from aggregating.	1185 at 0.2 C	500	Low attenuation of 0.07% per cycle	[108]
VO_2/VS_4/rGO/S	Vanadium–based VO_2/VS_4@RGO is prepared via tube furnace calcination and a one-step hydrothermal method. The vanadium-based heterostructures were electrostatically adsorbed onto the surface of 3D rGO.	771.94 at 2.0 C	700	Average decay rate of 0.071%	[109]
FeS_2-RGO-S/3D-Carbon fiber	A rational design of FeS_2-rGO and sulfur composite (FRHS) onto a 3D carbon fiber (CF) electrode as an efficient electrocatalyst and the conductive network for LiSBs.	1165 at 100 mA g^{-1}	325	73%	[110]
rGO/S/CF	A cathodic material (rGO_{150}/S/CF-75) was fabricated for Li-S batteries by adopting a melt-flow method to load sulfur on biomass-derived carbon fibers, then the rGO was electrochemically covered on the outside surface of the sulfur. The coverage of rGO layers endows the performance of S/CF-75 with multiple improvements.	1451.4 at 100 mA g^{-1}	1000	High at 5A g^{-1}	
MXene/rGO/C_3N_4 aerogel (MG/C_3N_4)/S	A MXene/rGO/C3N4 aerogel (MG/C_3N_4) with 3D-architecture prepared through a low-temperature hydrothermal approach followed by thermal treatment is used as a sulfur carrier for the free-standing cathode of Li-S batteries. In the MG/C_3N_4, MXene and rGO construct a highly conductive framework, and the MXene nanosheets offer chemical capture and catalytic activity towards lithium polysulfides in favor of good cycling stability. The introduction of g-C_3N_4 further enhances the reactivity of C-Ti-N at the hetero-interface by engineering the electronic state of Ti atoms, leading to the optimized metal d-band for expediting the multistep conversion of sulfur electrochemistry.	1315.6 at 0.2 C	100	97.5	[111]
CoN/Co_9S_8@rGO/S	The results of the first principal calculations, the catalytic effect, and the nucleation of the Li2S tests suggested that the CoN/Co_9S_8@rGO has strong chemical interaction, a fast conversion reaction kinetics, and catalytic effect of polysulfides, thereby inhibiting the leakage of the polysulfides.	1367.7 at 0.1 C	700	An extremely low decay rate of 0.06% per cycle and high cycling stability	[112]
A TiO_2-rGO heterostructure with abundant oxygen vacancies (H-TiO_2/rGO)	This rational structure provides sufficient active sites and lower bandgap for LiPSs and builds smooth adsorption-diffusion-conversion of LiPSs on the catalyst, reducing the interfacial energy barrier and enhancing sulfur utilization through the suppression of the destructive shuttling effect. With the synergetic properties of strong anchoring and catalyzing, the electrode (S-TiO_2/rGO) exhibits superior rate performance and long lifespan.		1000	0.023% capacity loss per cycle	[113]
Sulfur-functionalized rGO	This study presents a unique in-situ synthesis strategy to produce sulfur-functionalized rGO (SFRGO) encapsulating sulfur nanoparticles using a deep eutectic solvent (DES) from choline chloride and sodium thiosulfate. In addition to serving as a reducing agent, DES also serves as a doping agent. Furthermore, DES degrades to elemental sulfur during the formation of SFRGO.	1265	100	Capacity decay rate 0.28% each cycle	[114]
N-doped 3D interconnected-porous graphene (VN/N-rGO) hybrid architecture incorporating vanadium nitride (VN) nanoparticles	Typically, VN nanoparticles are derived from cracking and transformation of V_2O_5 nanowires, and their average size is below 20 nm. They provide abundant adsorption sites for sulfur species and facilitate a catalytic effect that accelerates the conversion of Li_2S_6 to Li_2S_2/Li_2S. Moreover, the interconnected highly conductive frameworks of N-rGO combined with abundant hierarchical pores enable fast electron/ion transport and polysulfides to be absorbed and entrapped.	698	200	78% at 1 C	[115]
CNT branched N-doped rGO networks encapsulating cobalt oxide nanoparticles	Using a simple pyrolysis method, a multidimensional architectured hybrid composed of porous N-rGO and CNT (Co@CNT/N-rGO) is synthesized. The composite exhibits a synergistic effect of homogeneously distributed Co_3O_4 nanoparticles, interconnected CNT branches, and a 3D hierarchical porous structure and N-doping that significantly suppresses the shuttle effect of lithium polysulfides. This enhances the redox kinetics of sulfur conversion.	1193.1 at 0.1 C	700	A low capacity fading rate of 0.030% per cycle	[116]
BN nanosheets wrapped by rGO	A distinctive 3D-microspheres composed of boron nitride (BN) nanosheets and rGO were applied to act as efficient sulfur cathode hosts for the first time in a spray-drying process. Using this construction, the robust microsphere structure could shorten ion diffusion pathways and supply sufficient spaces to alleviate the volumetric expansion of sulfur during lithiation. Besides, the synergistic effect between BN and rGO significantly enhanced polysulfide adsorption capability and accelerated their conversion, verified by the density functional theory (DFT) calculations and adsorption experiments.	1137 at 0.2 C	500	—	[117]

Table 3. Continued

Material	Description	Specific capacity (mAh g^{-1})	Number of cycles	Capacity retention (%)	Reference
3D S@MoS_2@rGO aerogels	Using 3D-MoS_2 nanoporous spheres (MoS_2-NPSs) decorated on conductive rGO as an S host, cathodes for S@MoS_2@GA were built.	668	500 cycles at 1.0 C	A low capacity fading rate of 0.054% per cycle	[118]
2D-rGO supported g-C_3N_4 (rGO/g-C_3N_4 QDs)	The C_3N_4 QDs with nanosizing can not only expose as many polysulfides adsorption sites to inhibit the "shuttle effect" and boost the kinetics but also possibly reduce its effect on rGO to achieve high S utilization and accelerate Li^+/charge transfer.	1013.9 at 1 C	500	A low capacity decay of 0.016% each cycle	[119]
TiN/rGO-Sulfur (TiN/rGO-S)	A microwave reduction strategy for synthesizing rGO-supported TiN nanoparticles hybrid (TiN/rGO). TiN/rGO-S show faster surface redox reaction kinetics, lower polarization, and enhanced stability cycling performance.	1197.6 at 0.1 C	150	—	[120]
Hollow $FePO_4$ spheres wrapped in rGO ($FePO_4$@rGO)	Sulfur is loaded into hollow $FePO_4$ spheres with large inner spaces, which buffer the volume expansion between S and discharge products (Li_2S/Li_2S_2) during cycling. As a result, the hollow and polar $FePO_4$ spheres provide synergistic physical confinement and chemical interaction to restrict the shuttle effect of polysulfides.	—	1000	Slow capacity fading rate of 0.037% per cycle at 0.5 C	[121]
Ni_3S_2 anchored to N/S co-doped rGO	A 3D-conductive network supports rapid charge transfer to the Ni3S2-polysulfide interface to improve the polysulfide's intrinsic equilibrium.	—	1000	A low capacity fading rate of 0.023% per cycle	[122]
Vertically grown *V*-MoS_2 onto *r*GO/S	In order to fabricate a self-supporting sulfur cathode using a nano storage-box structure (V-MoS_2 as the wall and rGO as the bottom), MoS_2 nanosheets were selectively grown vertically (V-MoS_2) on microwave-rGO sheets through chemical coupling. Carbon tubes can act as a long-range conductive path by connecting the abundant pores in the foam. As a result of the 2D-orthogonal-2D structure, the edge active sites of MoS_2 are maximally exposed. In conjunction with graphene, it forms a nanoreactor for sulfur, intermediate lithium polysulfides, and the discharge product Li_2S_2.	1379 at 0.1 C	500	86%	[123]
Graphene-based activated carbon composites/S	The synthesis of novel porous carbon composites combining activated carbons (ACs) within rGO is an appealing strategy that will help overcome the most limiting issues of LiSBs.	1100 mAh g^{-1} (3.90 mAh cm^{-2})	50	Capacity retention of >99.7% from the first to the last cycle at C/10	[124]
ZnS/rGO/S	A conformal zinc sulfide/reduced graphene oxide/elemental sulfur (ZnS/rGO/S) composite is synthesized as lithium-ion battery cathodes. As a result of regulating ohmic, concentration, and electrochemical polarization in synergistic ways, the overpotential of the Li‖ZnS/rGO/S cell is decreased and cycling performance is improved. The ZnS spheres absorb LiPSs intermediates, catalyze LiPSs conversion, and provide fast electronic/ionic diffusion kinetics, combining theoretical calculations and experimental results.	475	50	65	[125]
CoNiP quantum dot-decorated rGO	CoNiP-decorated graphene oxide (CoNiP-rGO) was developed and used as a sulfur host. The rGO disperses the CoNiP-QDs uniformly. As a result of the CoNiP-QDs and rGO, the CoNiP-rGO exhibits high specific capacity and cycle stability compared with CoP or NiP sulfur hosts.	598.2 at 3 C	600	A low capacity fading rate of 0.08% after 600 cycles at 1 C rate	[126]
rGO fiber cathodes containing polypyrrole@S nanospheres	In this study, polypyrrole@sulfur (PPy@S) nanospheres are homogenously implanted into the built-in cavity of self-assembled rGO fibers using a facile microfluidic assembly technique to enhance interface bonding and construct flexible fiber-shaped composite cathodes. Carbon and polymer interfaces host sulfur nanospheres and lithium polysulfides synergistically in this architecture. This improves the interface chemical bonding, resulting in good adsorption, fast reaction kinetics, and excellent mechanical flexibility for the cathode.	A high areal capacity of 5.8 mAh cm^{-2} at 0.2 A g^{-1}	—	—	[127]
Manganous oxide clusters (MOCs) in N-doped rGO	Sub-nanometric manganous oxide (MnO) clusters have been deposited in situ inside 2D-N-doped mesoporous carbon nanosheets using a composite micelle-directed assembly strategy.	990 mAh g^{-1} after 100 cycles at 0.2 A g^{-1}	100	60 over 250 cycles at 2.0 A g^{-1}	[128]
Tungsten oxide/zirconia (WO_3/ZrO_2)/rGO/S	WO_3/ZrO_2 pellets with a 3:1 ratio are prepared and incorporated into a 2D compacted Li_2S–graphene matrix. Combining graphene's high electrical conductivity with metastable high-pressure Li_2S phase allows the composite cathode to convert Li_2S directly into S_8 during its first activation process. As a polysulfide mediator, the tungsten oxide/zirconia particles block the outflow of soluble polysulfides into electrolyte solution by incorporating tungsten oxide/zirconia particles.	900 mAh g^{-1} at 0.1 C	1500	50 at 0.5 C	[129]
3D CoS_2/rGO aerogel/S	A 3D-conductive CoS_2/rGO is used as a trapping-catalyst sulfur host to improve LiSBs' performance. The rGO sheets are uniformly embedded with CoS_2, which traps LiPSs and then catalyzes its conversion. This inhibits the shuttle effect and accelerates reaction kinetics.	457 at 0.2 C	400	An ultra-low capacity fading rate per cycle of 0.04% at 1 C	[130]
Polypyrrole coated g-C_3N_4/rGO/S	A high-performance LiSB cathode was constructed using g-C_3N_4 and rGO composites polymerized with pyrrole (g-C_3N_4/rGO/S@PPy).	1189	200	91	[131]

Table 3. Continued

Material	Description	Specific capacity (mAh g^{-1})	Number of cycles	Capacity retention (%)	Reference
Janus Fe_3C/N-CNF@rGO	An electrode consisting of 1D-Fe_3C-decorated N-doped carbon nanofibers (Fe_3C/N-CNFs) and rGO was applied as a free-standing carrier for the Li_2S_6 catholyte to improve the overall electrochemical performance of LiSBs. The Fe_3C/N-CNF layer is capable of chemisorbing LiPSs and catalyzing LiPS conversion, which accelerates the redox kinetics. LiPSs are further inhibited from shuttling by the 2D-rGO sheets, which function as a microscopic physical barrier. By combining 1D-N-CNF sheets with 2D rGO sheets, the 3D-hierarchical conductive network enables fast electron transfer. It exhibits robust long-term cycling stability due to a synergetic effect of chemical immobilization, catalytic ability, and a physical barrier within a 3D-conductive network.	821.7 at 2.0 C	300	A low capacity fading rate of only 0.0089% per cycle at 0.5 C	[132]
Triphasic composite of LDH/sulfur/rGO	A triphasic material optimized for lithium-sulfur batteries with a crepe cake-like structure composed of LDH/sulfur/rGO. As sulfur nanoparticles are embedded in the interlayer spaces of the composite, they are well protected physically and chemically via 3D-wrapping and strong interactions between LDH nanoflakes and lithium polysulfides.	882 mAh g^{-1}, at 0.5 C	1000	80	[133]
A polyoxometalate framework ($[Co_4(PW_9O_{34})_2]^{10-}$) and multilayer rGO	This research involves the development of a molecular cluster catalyst composite composed of a polyoxometalate framework ($[Co_4(PW_9O_{34})_2]^{10-}$) and multilayer rGO. The composite demonstrates efficient polysulfide adsorption and reduced activation energy for polysulfide conversion, enabling it to function as a bifunctional electrocatalyst.	800 mAh g^{-1}	1000	A low capacity decay rate of 0.015% per cycle	[134]
3D-rGO-encapsulated SnO_2 nanoparticles/(SnO_2/rGO)	The rational design of graphene-encapsulated nanomaterials is of great significance to the high-rate and long-cycle anode materials in lithium-ion batteries. Herein, composites of three-dimensional reduced graphene oxide-encapsulated SnO_2 nanoparticles (SnO_2/rGO) have been synthesized by combining hydrothermal treatment with spray drying or freeze drying and calcination.	1592 mAh g^{-1} after 500 cycles at 500 mA g^{-1}	500	It can maintain 319 mAh g^{-1} even at 5 A g^{-1}	[135]
Hollow MoS_2 nanocages rGO sheets (H-MoS_2/rGO)	H-MoS_2/rGO composites are found to be potential hosts for S cathodes in LiSBs. rGO sheets are covered with hollow MoS_2 nanocages tightly bound by C-O-Mo bonds. MoS_2 nanocages adsorb polysulfides via the Mo-S bond and accelerate the conversion of S_8 into Li_2S.	801.7 mAh g^{-1} at 1 C	500	—	[136]
Microassemblies of graphene decorated with Ni_2Co nanoalloys (Ni_2Co@rGO)	An advanced S host matrix for Li-S batteries has been developed with Ni_2Co@rGO. Based on computational, physicochemical, and electrochemical studies, Ni_2Co nanoalloys have excellent catalytic activity for sulfur conversion and strong adsorption ability against polysulfide shuttling. In addition, the sophisticated architecture enables the highly exposed active interfaces.	An areal capacity of 4.53 mAh cm^{-2}	500	A low capacity fading of 0.034% per cycle	[137]
S/Fe@rGO	Fe-rGO/S as a cathode material for high-performance LiSBs	1634.3	200	—	[138]
3D-Graphene/WO_3 nanowire composite	A 3D-hierarchical structure of rGO-WO_3 as a sulfur host material in LiSBs. In-situ electrochemical studies and computational methods showed that the rGO@WO_3 can catalyze the LiPSs conversion to improve LiSB's performance.	1410 at 0.1 C	500	A low capacity fading rate of 0.086% per cycle	[139]
rGO/CNT composite sulfur hosts	This work used ammonia and hydrazine hydrate as nitrogen source precursors to prepare three kinds of rGO and CNT composite sulfur hosts with different nitrogen configurations. Ammonia is conducive to the formation of Pyrrolic N. At the same time, hydrazine hydrate is conducive to forming Pyridinic N. Lithium-sulfur batteries assembled with 3NG/CNT/S, which has similar Pyridinic N and Pyrrolic N contents.	1345 mAh g^{-1} at 0.2 C	400	819 mAh g^{-1} after 400 cycles at 2 C	[140]
Multicarbonyl perylene-based organic molecule (PN)/rGO/S	PN-rGO composite networks were formed using perylene-based organic molecules with multiple carbonyl groups (PN). It is possible for PN with a large conjugated planar structure to be highly distributed throughout the electrode. The rGO provides PN molecules with a substrate and could prevent them from aggregating. PN can also effectively adsorb polysulfide through S-O interaction, reducing the shuttle effect of polysulfide.	1071 at 0.2 C	200	—	[141]
Sulfurized polyacrylonitrile grafted rGO(S-PAN)-*g*-rGO	A sulfur cathode in the form of a unique bamboo-shaped structured nanofiber uses SPAN as the bamboo stalk and rGO as the bamboo joint, thus ensuring that the S-PAN has excellent electronic conductivity. Polyacrylonitrile grafted with rGO (PAN-*g*-rGO) is an effective composite of ultra-high molecular weight PAN (UHMW PAN) and rGO at the molecular level. The UHMW PAN precursor can provide high sulfur loading. Sulfurized PAN-*g*-rGO fiber (SFPAN-*g*-rGO) with a sulfur content of approximately 53 wt% is fabricated using PAN-*g*-rGO with a molecular weight of 3.6×10^5 Da as the precursor.	1463 mAh g^{-1} at 0.2 C	800 cycles	—	[142]

Acknowledgements

This research was funded by the Alfaisal University grant number 726174. The authors gratefully acknowledge the Alfaisal University and its Office of Research and Innovation for their continuous support throughout this study.

Conflict of Interest

The authors declare no conflict of interest.

Data Availability Statement

No experimental data is associated with this manuscript.

Keywords

energy storage, graphene, graphene oxide, lithium-sulfur battery, nanocomposites

Received: February 16, 2025
Revised: April 8, 2025
Published online: April 15, 2025

[1] V. K. Tomer, R. Malik, J. Tjong, M. Sain, *Coord. Chem. Rev.* **2023**, *481*, 215055.
[2] T.-Z. Ang, M. Salem, M. Kamarol, H. S. Das, M. A. Nazari, N. Prabaharan, *Energ. Strat. Rev.* **2022**, *43*, 100939.
[3] S. O. Ganiyu, C. A. Martinez-Huitle, *Curr. Opin. Electrochem.* **2020**, *22*, 211.
[4] R. Jain, A. S. Lakhnot, K. Bhimani, S. Sharma, V. Mahajani, R. A. Panchal, M. Kamble, F. Han, C. Wang, N. Koratkar, *Nat. Rev. Mater.* **2022**, *7*, 736.
[5] M. Fichtner, K. Edström, E. Ayerbe, M. Berecibar, A. Bhowmik, I. E. Castelli, S. Clark, R. Dominko, M. Erakca, A. A. Franco, A. Grimaud, B. Horstmann, A. Latz, H. Lorrmann, M. Meeus, R. Narayan, F. Pammer, J. Ruhland, H. Stein, T. Vegge, M. Weil, *Adv. Energy Mater.* **2022**, *12*, 2102904.
[6] L. Mauler, F. Duffner, W. G. Zeier, J. Leker, *Energ. Environ. Sci.* **2021**, *14*, 4712.
[7] T. Palit, A. B. M. M. Bari, C. L. Karmaker, *Decis. Anal. J.* **2022**, *4*, 100119.
[8] K. J. Shah, S. Y. Pan, I. Lee, H. Kim, Z. You, J. M. Zheng, P. C. Chiang, *J. Clean. Prod.* **2021**, *326*, 129392.
[9] P. Barman, L. Dutta, S. Bordoloi, A. Kalita, P. Buragohain, S. Bharali, B. Azzopardi, *Renew. Sustain. Energy Rev.* **2023**, *183*, 113518.
[10] M.-T. Lee, W.-N. Su, *Appl. Sci.* **2020**, *10*, 952.
[11] P. V. Chombo, Y. Laoonual, *J. Power Sources* **2020**, *478*, 228649.
[12] Q. Zhang, J. Niu, Z. Zhao, Q. Wang, *J. Energy Storage* **2022**, *45*, 103759.
[13] C. Heubner, M. Schneider, A. Michaelis, *Adv. Energy Mater.* **2020**, *10*, 1902523.
[14] Y. Chen, T. Wang, H. Tian, D. Su, Q. Zhang, G. Wang, *Adv. Mater.* **2021**, *33*, 2003666.
[15] T. Wang, J. He, X. B. Cheng, J. Zhu, B. Lu, Y. Wu, *ACS Energy Lett.* **2022**, *8*, 116.
[16] R. Deng, M. Wang, H. Yu, S. Luo, J. Li, F. Chu, B. Liu, F. Wu, *Energy Environ. Mater.* **2022**, *5*, 777.
[17] Z. Han, S. Li, Y. Wu, C. Yu, S. Cheng, J. Xie, *J. Mater. Chem. A* **2021**, *9*, 24215.
[18] S. Ohno, W. G. Zeier, *Acc. Mater. Res.* **2021**, *2*, 869.
[19] B. Ding, J. Wang, Z. Fan, S. Chen, Q. Lin, X. Lu, H. Dou, A. Kumar Nanjundan, G. Yushin, X. Zhang, Y. Yamauchi, *Mater. Today* **2020**, *40*, 114.
[20] L. Huang, J. Li, B. Liu, Y. Li, S. Shen, S. Deng, C. Lu, W. Zhang, Y. Xia, G. Pan, X. Wang, Q. Xiong, X. Xia, J. Tu, *Adv. Funct. Mater.* **2020**, *30*, 1910375.
[21] G. Liu, Q. Sun, Q. Li, J. Zhang, J. Ming, *Energy Fuel* **2021**, *35*, 10405.
[22] S. Zeng, G. M. Arumugam, X. Liu, Y. Yang, X. Li, H. Zhong, F. Guo, Y. Mai, *Small* **2020**, *16*, e2001027.
[23] S. Li, Z. Fan, *Energy Storage Mater.* **2021**, *34*, 107.
[24] M. Nojabaee, B. Sievert, M. Schwan, J. Schettler, F. Warth, N. Wagner, B. Milow, K. A. Friedrich, *J. Mater. Chem. A* **2021**, *9*, 6508.
[25] X. Ji, S. Evers, K. T. Lee, L. F. Nazar, *Chem. Commun.* **2010**, *46*, 1658.
[26] Y. Xiang, L. Lu, A. G. P. Kottapalli, Y. Pei, *Carbon Energy* **2022**, *4*, 346.
[27] N. Deng, X. Feng, Y. Jin, Z. Peng, Y. Feng, Y. Tian, Y. Liu, L. Gao, W. Kang, B. Cheng, *J. Energy Chem.* **2024**, *89*, 266.
[28] S. Zhang, R. Shi, K. Cai, T. Wang, T. Qu, L. Li, X. Lang, *J. Electroanal. Chem.* **2024**, *967*, 118468.
[29] M. J. Klein, A. Dolocan, C. Zu, A. Manthiram, *Adv. Energy Mater.* **2017**, *7*, 1701122.
[30] X. Liu, J. Rahmatinejad, Z. Ye, *Chem. Eng. J.* **2021**, *422*, 130129.
[31] H. Chen, W. D. Dong, F. J. Xia, Y. J. Zhang, M. Yan, J. P. Song, W. Zou, Y. Liu, Z. Y. Hu, J. Liu, Y. Li, H. E. Wang, L. H. Chen, B. L. Su, *Chem. Eng. J.* **2020**, *381*, 122746.
[32] J. Yang, H. J. Han, H. Repich, R. C. Zhi, C. Z. Qu, L. Kong, S. Kaskel, H. Q. Wang, F. Xu, H. J. Li, *New Carbon Mater.* **2020**, *35*, 630.
[33] Y. Bai, T. Li, Y. Wang, H. Jin, K. Wang, H. Xu, *Int. J. Energy Res.* **2020**, *44*, 70.
[34] L. Zhang, Y. Wang, Z. Niu, J. Chen, *Carbon* **2019**, *141*, 400.
[35] J. Park, S. H. Yu, Y. E. Sung, *Nano Today* **2018**, *18*, 35.
[36] Z. Wei, S. Sarwar, X. Zhang, R. Wang, *J. Colloid Interface Sci.* **2025**, *678*, 210.
[37] Z. Wei, S. Sarwar, S. Azam, M. R. Ahasan, M. Voyda, X. Zhang, R. Wang, *J. Colloid Interface Sci.* **2023**, *635*, 391.
[38] Y. Lan, Y. Wang, G. Lu, L. Liu, T. Tang, M. Li, Y. Cheng, J. Xiao, X. Li, *ACS Nano* **2024**, *18*, 15638.
[39] C.-C. Chuang, Y. Y. Hsieh, W. C. Chang, H. Y. Tuan, *Chem. Eng. J.* **2020**, *387*, 123904.
[40] Y. Ning, B. Wang, F. Jin, J. Yang, J. Zhang, H. Luo, F. Wu, Z. Zhang, H. Zhang, Y. Zhou, D. Wang, *J. Alloys Compd.* **2020**, *838*, 155504.
[41] D. Ying, X. Yu, X. Liu, C. Ma, W. Qiao, J. Wang, L. Ling, *Energy Fuel* **2024**, *38*, 9080.
[42] J. Pu, W. Gong, Z. Shen, L. Wang, Y. Yao, G. Hong, *Adv. Sci.* **2022**, *9*, e2104375.
[43] H. Kim, J. Y. Hwang, S. Bang, H. G. Jung, Y. K. Sun, *J. Mater. Chem. A* **2022**, *10*, 10844.
[44] H. Liu, F. Liu, Z. Qu, J. Chen, H. Liu, Y. Tan, J. Guo, Y. Yan, S. Zhao, X. Zhao, X. Nie, X. Ma, Z. Pei, M. Liu, *Nano Res. Energy* **2023**, *2*, e9120049.
[45] C. C. Zuluaga-Gómez, C. O. Plaza-Rivera, B. Tripathi, R. K. Katiyar, D. K. Pradhan, G. Morell, Y. Lin, M. Correa, R. S. Katiyar, *ACS Omega* **2023**, *8*, 13097.
[46] X. Liu, Q. He, J. Liu, R. Yu, Y. Zhang, Y. Zhao, X. Xu, L. Mai, L. Zhou, *ACS Appl. Mater. Interfaces* **2023**, *15*, 9439.
[47] L. Sun, Y. Liu, J. Xie, L. Fan, J. Wu, R. Jiang, Z. Jin, *Chem. Eng. J.* **2023**, *451*, 138370.
[48] L. Zhou, R. Gao, T. Wang, J. Liu, T. Yan, X. P. Gao, *ACS Appl. Energy Mater.* **2024**, *7*, 7338.
[49] L. C. Greenburg, X. Gao, P. Zhang, X. Zheng, J. Wang, R. A. Vilá, Y. Cui, *Nano Lett.* **2023**, *23*, 5967.
[50] T. Wang, Q. Zhang, J. Zhong, M. Chen, H. Deng, J. Cao, L. Wang, L. Peng, J. Zhu, B. Lu, *Adv. Energy Mater.* **2021**, *11*, 2100448.

[51] J. Zhang, G. Xu, Q. Zhang, X. Li, Y. Yang, L. Yang, J. Huang, G. Zhou, *Adv. Sci.* **2022**, *9*, 2201579.
[52] H. Ci, J. Cai, H. Ma, Z. Shi, G. Cui, M. Wang, J. Jin, N. Wei, C. Lu, W. Zhao, J. Sun, Z. Liu, *ACS Nano* **2020**, *14*, 11929.
[53] I. Tantis, A. Bakandritsos, D. Zaoralová, M. Medveď, P. Jakubec, J. Havláková, R. Zbořil, M. Otyepka, *Adv. Funct. Mater.* **2021**, *31*, 2101326.
[54] J. Guo, H. Jiang, X. Li, Z. Chu, W. Zheng, Y. Dai, X. Jiang, X. Wu, G. He, *Energy Storage Mater.* **2021**, *40*, 358.
[55] Z. Cheng, Y. Chen, Y. Yang, L. Zhang, H. Pan, X. Fan, S. Xiang, Z. Zhang, *Adv. Energy Mater.* **2021**, *11*, 2003718.
[56] P. Yu, L.-X. Feng, D.-C. Ma, X.-R. Sun, J.-K. Pei, X.-J. Zha, R.-Y. Bao, Y. Wang, M.-B. Yang, Z.-P. Guo, W. Yang, *Adv. Funct. Mater.* **2021**, *31*, 2008652.
[57] E. Jing, L. Chen, S. Xu, W. Tian, D. Zhang, N. Wang, Z. Bai, X. Zhou, S. Liu, D. Duan, X. Qiu, *J. Energy Chem.* **2022**, *64*, 574.
[58] F. Li, M. Zhang, W. Chen, X. Cai, H. Rao, J. Chang, Y. Fang, X. Zhong, Y. Yang, Z. Yang, X. Yu, *ACS Appl. Mater. Interfaces* **2021**, *13*, 30746.
[59] Y. Jia, Y. S. Zhao, X. X. Yang, M. X. Ren, Y. Q. Wang, B. Y. Lei, D. L. Zhao, *Int. J. Hydrogen Energy* **2021**, *46*, 7642.
[60] L. Gong, R. Yang, R. Liu, Y. Zou, Y. Liu, L. Chen, Y. Yan, Y. Xu, *J. Alloys Compd.* **2021**, *855*, 157278.
[61] S. Zhang, P. Zhang, R. Hou, B. Li, Y. Zhang, K. Liu, X. Zhang, G. Shao, *J. Energy Chem.* **2020**, *47*, 281.
[62] S. Niu, S. W. Zhang, R. Shi, J. Wang, W. Wang, X. Chen, Z. Zhang, J. Miao, A. Amini, Y. Zhao, C. Cheng, *Energy Storage Mater.* **2020**, *33*, 73.
[63] M. Zhang, L. Wang, B. Wang, B. Zhang, X. Sun, D. Wang, Z. Kong, L. Xu, *J. Mater. Chem. A* **2021**, *9*, 6538.
[64] M. Li, X. Zhou, X. Ma, L. Chen, D. Zhang, S. Xu, D. Duan, C. Chen, Q. Yuan, S. Liu, *Chem. Eng. J.* **2021**, *409*, 128164.
[65] W. Chen, H. Jin, S. Xie, H. Xie, J. Zhu, H. Ji, L. J. Wan, *J. Energy Chem.* **2021**, *54*, 16.
[66] J. Jin, W. Cai, J. Cai, Y. Shao, Y. Song, Z. Xia, Q. Zhang, J. Sun, *J. Mater. Chem. A* **2020**, *8*, 3027.
[67] J. Tan, D. Li, Y. Liu, P. Zhang, Z. Qu, Y. Yan, H. Hu, H. Cheng, J. Zhang, M. Dong, C. Wang, J. Fan, Z. Li, Z. Guo, M. Liu, *J. Mater. Chem. A* **2020**, *8*, 7980.
[68] X. Wen, K. Xiang, Y. Zhu, L. Xiao, H. Liao, W. Chen, X. Chen, H. Chen, *J. Alloys Compd.* **2020**, *815*, 152350.
[69] B. Wang, F. Jin, Y. Xie, H. Luo, F. Wang, T. Ruan, D. Wang, Y. Zhou, S. Dou, *Energy Storage Mater.* **2020**, *26*, 433.
[70] L. Lu, F. Pei, T. Abeln, Y. Pei, *Carbon* **2020**, *157*, 437.
[71] H. Xu, Q. Jiang, B. Zhang, C. Chen, Z. Lin, *Adv. Mater.* **2020**, *32*, e1906357.
[72] A. E. Baumann, J. R. Downing, D. A. Burns, M. C. Hersam, V. S. Thoi, *ACS Appl. Mater. Interfaces* **2020**, *12*, 37173.
[73] J. Li, X. Li, X. Fan, T. Tang, M. Li, Y. Zeng, H. Wang, J. Wen, J. Xiao, *Carbon* **2022**, *188*, 155.
[74] J. Lin, Y. Mo, S. Li, J. Yu, *J. Mater. Chem. A* **2022**, *10*, 690.
[75] B. C. Xian, S. Shen, T. Yang, Z. Qiu, Y. Zhang, F. Cao, X. Liang, M. Chen, X. He, Y. Xia, C. Wang, W. Wan, W. Zhang, X. Xia, J. Tu, J. Zhou, *ACS Nano* **2024**, *18*, 27451.
[76] X. Li, Y. Yu, Z. Tang, Y. Yang, Y. Li, J. Cao, L. Chen, *Phys. Chem. Chem. Phys.* **2022**, *24*, 2879.
[77] H.-J. Li, Y. H. Song, K. Xi, W. Wang, S. Liu, G. R. Li, X. P. Gao, *J. Mater. Chem. A* **2021**, *9*, 10704.
[78] C. C. Zuluaga-Gómez, B. Tripathi, C. O. Plaza-Rivera, R. K. Katiyar, M. Correa, D. K. Pradhan, G. Morell, R. S. Katiyar, *Batteries* **2023**, *9*, 293.
[79] P. Ponmani, J. Bahadur, C. Tewari, D. K. Gupta, U. Kalita, P. Jegadeesan, T. R. Ravindran, A. Alex, A. Das, N. Sahoo, M. Sivanantham, S. Choudhury, *J. Polym. Sci.* **2023**, *61*, 2149.
[80] X. Zhang, T. Wan, A. Jia, J. Li, G. Liu, D. Sun, Y. Wang, *Electrochim. Acta* **2021**, *397*, 139264.
[81] N. Badi, A. S. Roy, H. A. Al-Aoh, S. A. Alghamdi, A. S. Alatawi, A. A. Alatawi, A. Ignatiev, *Mater. Sci. Energy Technol.* **2023**, *6*, 351.
[82] Y. Ma, X. Zhou, X. Liu, X. Ma, J. Du, D. Duan, L. Chen, Q. Yuan, S. Liu, *J. Electroanal. Chem.* **2024**, *954*, 118041.
[83] F. Han, D. Yan, X. Guan, Q. Lu, S. Yin, Y. Yan, H. Zhou, P. Yang, Q. Zhang, S. Zhang, J. Xia, Y. Xing, *Energy Storage Mater.* **2024**, *71*, 103652.
[84] M. Xu, T. Wang, H. Wang, Y. Wang, S. Li, J. Sun, J. Sha, *Inorg. Chem.* **2023**, *62*, 3134.
[85] Z. Shi, R. Du, C. Yu, M. Shi, C. Xu, J. Wang, R. Ren, *Mater. Lett.* **2024**, *354*, 135392.
[86] J. Wei, B. Chen, H. Su, C. Jiang, X. Li, S. Qiao, H. Zhang, *Ceram. Int.* **2021**, *47*, 2686.
[87] Z. Li, Z. Wu, M. Bi, H. Yu, C. Ma, J. Xiang, S. Yao, *J. Mater. Sci. Mater. Electron.* **2022**, *33*, 12871.
[88] Z. Hu, G. Yan, J. Zhao, X. Zhang, Y. Feng, X. Qu, H. Ben, J. Shi, *Nanotechnology* **2022**, *33*, 225402.
[89] R. Saroha, H. S. Ka, G. D. Park, C. Cho, D. W. Kang, J. S. Cho, *J. Power Sources* **2024**, *592*, 233893.
[90] S. Suriyakumar, G. J. Rani, A. M. Stephan, *Ionics* **2020**, *26*, 2201.
[91] G. Chen, J. Li, N. Liu, Y. Zhao, J. Tao, G. Kalimuldina, Z. Bakenov, Y. Zhang, *Electrochim. Acta* **2019**, *326*, 134968.
[92] W. I. Kim, J. S. Yeon, H. Park, H. J. Kim, M. J. Kim, J. Kim, H. S. Park, *Compos. B Eng.* **2023**, *264*, 110886.
[93] Y. Zhang, Y. Dong, X. Yan, H. Peng, S. Xu, M. Zhu, Z. Jin, L. Han, J. Zhang, *J. Energy Storage* **2024**, *84*, 111023.
[94] N. Cyril Karima, S. Jin, S. Mook Choi, K. Jenerali Nyamtara, P. Maldonado Nogales, M. Cuong Nguyen, S. Hoon Kim, S. Nam Lim, S. K. Jeong, H. K. Kim, M. Ho Seo, W. Ahn, *Chem. Eng. J.* **2024**, *497*, 154634.
[95] G. R. Deivendran, M. Seenivasan, Y.-S. Wu, J.-K. Chang, R. Jose, M. Poddar, C.-L. Sun, C.-C. Yang, *ACS Sustain. Chem. Eng.* **2024**, *12*, 14553.
[96] B. Chen, J. Wei, X. Li, Y. Ji, D. Liang, T. Chen, *J. Colloid Interface Sci.* **2023**, *629*, 1003.
[97] J. M. Park, S. H. Baek, W. I. Kim, S. J. Lee, G. S. Gund, H. S. Park, *Electrochim. Acta* **2023**, *462*, 142750.
[98] X. Zhao, Y. Dang, H. Ma, P. Bai, W. Li, Z. H. Liu, *Inorg. Chem.* **2024**, *63*, 3107.
[99] Y. Huang, Y. Chen, X. Song, Q. Q. Liu, X. X. Lu, Q. Jiang, *Mater. Today Chem.* **2023**, *30*, 101592.
[100] Z. Wang, C. Cui, Y. Zhao, H. Li, T. Wu, Z. Zhao, J. Wei, *Energy Fuel* **2023**, *37*, 12457.
[101] R. Colombo, D. Versaci, J. Amici, F. Bella, M. L. Para, N. Garino, M. Laurenti, S. Bodoardo, C. Francia, *Nanomaterials* **2023**, *13*, 2149.
[102] Y. Shi, K. Zhang, H. Wang, T. Wan, L. Wu, G. Liu, *J. Alloys Compd.* **2023**, *968*, 172059.
[103] K. S. Rao, D. D. Pathak, B. P. Mandal, S. Kumar, A. K. Tyagi, *Mater. Today Commun.* **2023**, *36*, 106708.
[104] M. Li, H. Chen, C. Guo, S. Qian, H. Li, Z. Wu, C. Xing, P. Xue, S. Zhang, *Adv. Energy Mater.* **2023**, *13*, 2300646.
[105] Z. Li, J. Liu, T. Wang, J. Zhu, C. Cheng, G. Ao, Z. Guan, J. Zhu, *Carbon* **2024**, *222*, 118966.
[106] Y. Lu, H. Yao, W. Gao, A. Jia, Y. Lu, Y. Yu, J. He, Y. Wu, *Compos. Commun.* **2024**, *49*, 101981.
[107] P. B. Nagy, L. Shiva Shankar, M. Szabados, H. Roumia, Á. Kukovecz, R. Kun, T. Szabó, *J. Colloid Interface Sci.* **2024**, *655*, 931.
[108] T. Zhang, Z. Xu, H. Chen, J. Liu, D. Luo, N. Liu, Y. Zhang, Z. Chen, *Chem. Eng. J.* **2024**, *488*, 150886.
[109] P. Lin, B. Gao, J. Li, H. Fu, X. Lan, Z. Liu, M. Wang, H. Zhang, *Diamond Relat. Mater.* **2024**, *147*, 111287.
[110] J. P. Grace, S. K. Martha, *J. Energy Storage* **2024**, *88*, 111585.
[111] B. Yang, M. Xu, Y. Gao, Q. Zhu, B. Xu, *Small Methods* **2024**, *8*, 2301102.
[112] Y. Tang, Y. Yuan, Y. Mo, H. Tang, M. Wei, H. Zhou, T. Sheng, C. Li, Y. Sun, X. Wei, *Mater. Today Phys.* **2024**, *46*, 101480.
[113] Y. Feng, H. Liu, Y. Liu, F. Zhao, J. Li, X. He, *J. Energy Chem.* **2021**, *62*, 508.

[114] P. H. Wadekar, A. Ghosh, R. V. Khose, D. A. Pethsangave, S. Mitra, S. Some, *Electrochim. Acta* **2020**, *344*, 136147.
[115] N. Li, Z. Xu, P. Wang, Z. Zhang, B. Hong, J. Li, Y. Lai, *Chem. Eng. J.* **2020**, *398*, 125432.
[116] J. S. Yeon, Y. H. Ko, T. H. Park, H. Park, J. Kim, H. S. Park, *Energy Environ. Mater.* **2022**, *5*, 555.
[117] W. Gao, Y. Liu, C. Cao, Y. Zhang, Y. Xue, C. Tang, *J. Colloid Interface Sci.* **2022**, *610*, 527.
[118] Y. Hou, Y. Ren, S. Zhang, K. Wang, F. Yu, T. Zhu, *J. Alloys Compd.* **2021**, *852*, 157011.
[119] D. Zhao, Z. Xu, X. Yu, M. Chen, O. Wu, K. Zhou, W. Zhou, L. Ma, N. Wang, *Chem. Eng. J.* **2023**, *474*, 145983.
[120] J. Tu, H. Li, T. Lan, S. Z. Zeng, J. Zou, Q. Zhang, X. Zeng, *J. Alloys Compd.* **2020**, *822*, 153751.
[121] C. Huang, Y. Zhou, H. Shu, M. Chen, Q. Liang, S. Jiang, X. Li, T. Sun, M. Han, Y. J. Zhou, J. Jian, X. Wang, *Electrochim. Acta* **2020**, *329*, 135135.
[122] D. Guo, Z. Zhang, B. Xi, Z. Yu, Z. Zhou, X. A. Chen, *J. Mater. Chem. A* **2020**, *8*, 3834.
[123] B. Cui, X. Cai, W. Wang, P. Saha, G. Wang, *J. Energy Chem.* **2022**, *66*, 91.
[124] G. Jiménez-Martín, J. Castillo, X. Judez, J. L. Gómez-Urbano, G. Moreno-Fernández, A. Santiago, A. de Saenz Buruaga, I. Garbayo, J. A. Coca-Clemente, A. Villaverde, M. Armand, C. Li, D. Carriazo, *Batter. Supercaps* **2022**, *5*, e202200167.
[125] H. Peng, Y. Zhang, Y. Chen, J. Zhang, H. Jiang, X. Chen, Z. Zhang, Y. Zeng, B. Sa, Q. Wei, J. Lin, H. Guo, *Mater. Today Energy* **2020**, *18*, 100519.
[126] T. Xiao, F. Yi, M. Yang, W. Liu, M. Li, M. Ren, X. Zhang, Z. Zhou, *J. Mater. Chem. A* **2021**, *9*, 16692.
[127] L. Huang, T. Guan, H. Su, Y. Zhong, F. Cao, Y. Zhang, X. Xia, X. Wang, N. Bao, J. Tu, *Angew. Chem.* **2022**, *61*, e202212151.
[128] P. Qiu, Y. Yao, W. Li, Y. Sun, Z. Jiang, B. Mei, L. Gu, Q. Zhang, T. Shang, X. Yu, J. Yang, Y. Fang, G. Zhu, Z. Zhang, X. Zhu, T. Zhao, W. Jiang, Y. Fan, L. Wang, B. Ma, L. Liu, Y. Yu, W. Luo, *Nano Lett.* **2021**, *21*, 700.
[129] Z. Zhao, R. Pathak, X. Wang, Z. Yang, H. Li, Q. Qiao, *Electrochim. Acta* **2020**, *364*, 137117.
[130] Y. Li, J. Li, J. Yuan, Y. Zhao, J. Zhang, H. Liu, F. Wang, J. Tang, J. Song, *J. Alloys Compd.* **2021**, *873*, 159780.
[131] S.-H. Moon, J. H. Shin, J. H. Kim, J. S. Jang, S. B. Kim, Y. Y. Park, S. N. Lee, K. W. Park, *Mater. Chem. Phys.* **2022**, *287*, 126267.
[132] J. Li, H. Zhang, L. Luo, H. Li, J. He, H. Zu, L. Liu, H. Liu, F. Wang, J. Song, *J. Mater. Chem. A* **2021**, *9*, 2205.
[133] S. Liu, X. Zhang, S. Wu, X. Chen, X. Yang, W. Yue, J. Lu, W. Zhou, *ACS Nano* **2020**, *14*, 8220.
[134] J. Lei, X. X. Fan, T. Liu, P. Xu, Q. Hou, K. Li, R. M. Yuan, M. S. Zheng, Q. F. Dong, J. J. Chen, *Nat. Commun.* **2022**, *13*, 202.
[135] Z. Lu, Z. Kong, L. Jing, T. Wang, X. Liu, A. Fu, P. Guo, Y. G. Guo, H. Li, *Energy Fuel* **2020**, *34*, 13126.
[136] J. Lu, Y. Chen, Y. Zhang, J. Huang, H. Jiang, D. He, H. Chen, *J. Alloys Compd.* **2024**, *1004*, 175674.
[137] G. Li, W. Qiu, W. Gao, Y. Zhu, X. Zhang, H. Li, Y. Zhang, X. Wang, Z. Chen, *Adv. Funct. Mater.* **2022**, *32*, 2202853.
[138] J. Yao, M. Zhang, G. Han, X. Wang, Z. Wang, J. Wang, *Ceram. Int.* **2020**, *46*, 24155.
[139] L. Ni, S. Duan, H. Zhang, J. Gu, G. Zhao, Z. Lv, G. Yang, Z. Ma, Y. Liu, Y. Fu, Z. Wu, J. Xie, M. Chen, G. Diao, *Carbon* **2021**, *182*, 335.
[140] W. Dong, Z. Wu, X. Zhu, D. Shen, M. Zhao, F. Yang, Q. Chang, S. Tang, X. Hong, Z. Dong, S. Yang, *Chem. Eng. J.* **2024**, *488*, 150872.
[141] G. Huang, K. Jia, X. Li, J. Zhang, Y. Luo, C. Zhong, L. Zhu, F. Wu, *Appl. Surf. Sci.* **2023**, *615*, 156430.
[142] H. Liu, R. He, Y. Li, Y. Jin, H. Liu, X. Zhang, *J. Electroanal. Chem.* **2023**, *939*, 117465.
[143] W. Deng, J. Phung, G. Li, X. Wang, *Nano Energy* **2021**, *82*, 105761.